IEEE Open Journal of
Power Electronics

Received 29 June 2021; revised 30 July 2021; accepted 5 August 2021. Date of publication 12 August 2021;
date of current version 15 September 2021. The review of this article was arranged by Associate Editor Tommaso Caldognetto.

Digital Object Identifier 10.1109/OJPEL.2021.3104502

Two-Port Characterization and Transfer Immittances of AC-DC Converters—Part I: Modeling

JIAN SUN (Fellow, IEEE)

Department of Electrical, Computer, and Systems Engineering, Rensselaer Polytechnic Institute, Troy, NY 12180 USA

ABSTRACT This two-part paper presents a general method to model three-phase ac-dc converters in the frequency domain for power system stability studies. In the developed approach, an ac-dc converter is treated as a two-port network connecting an ac and a dc power system, and is characterized by a set of self and transfer immittances. The transfer immittances describe two types of small-signal coupling that are unique to three-phase ac-dc converters: The first type describes the coupling between the ac and dc port and involves a frequency shift by the fundamental; the second type models the coupling over frequency in the ac port current response and involves a frequency shift by twice the fundamental. Together with the self-immittances of each port, the developed models can be used as building blocks to support impedance-based stability analysis of various power systems that involve such converters, including ac, dc, and hybrid ac-dc power generation, transmission and distribution systems. Part I of the paper explains the two-port modeling approach and develops the associated models for a two-level voltage-source converter. Part II presents applications of the developed models for stability analysis of different systems.

INDEX TERMS Ac-dc power conversion, frequency domain analysis, power system, stability, two-port circuits.

I. INTRODUCTION

Small-signal characterization of power converters at their terminals is the foundation for system stability analysis. Terminal characteristics of dc-dc converters have been studied since the 1970s. The impedance-based approach originally developed in [1] for studying converter-filter interactions has evolved into a general method for stability analysis of dc power electronics systems, including space and satellite power systems that were the focus of early research [2], as well as dc distributed power systems [3] and dc microgrids [4] in more recent years. In addition to input and output impedances, modeling of dc-dc converters as two-port networks using Y (admittance) and H (hybrid) parameters have also been proposed [2]. Key to these successful developments and applications is a systematic method to model dc-dc converters based on averaging and linearization [8].

A. AC-DC CONVERTERS AND THEIR MODELING

Converters performing power conversion from ac to dc or dc to ac have been traditionally called ac-dc converters and dc-ac converters, respectively. The different names have been used to indicate the different directions of power flow through the converter. This naming convention becomes ambiguous in applications where the power flow is bidirectional. To avoid confusion, we will refer to both types collectively as *ac-dc converters* in this work regardless of power flow direction. Accordingly, the terminals of such a converter will be called the ac and dc port (or terminal) instead of input and output. The ac port may be single-phase or three-phase in general. This work focuses on three-phase ac-dc converters.

Compared to the modeling of dc-dc converters, small-signal terminal characterization of ac-dc converters did not draw much attention until recent years. Early work in this area was limited to input impedance modeling of PWM rectifiers [5]–[7]. A principal difficulty with small signal modeling of ac-dc converters in general is the periodical variation of voltage, current and control at the fundamental frequency. Direct linearization of such a converter model leads to a linear time-periodic (LTP) model that is difficult to work with in practice. The input impedance model presented in [5] for single-phase

power factor correction (PFC) converters avoided this difficulty by treating the dc bus as an ideal voltage source, which effectively rendered the converter model linear, thereby avoiding the need for linearization. The method proposed in [6] and [7] for three-phase PWM rectifiers used dq transformation to remove time-periodic variables and develop models in a dq reference frame that rotates synchronously with the converter terminal voltage.

The work on impedance modeling of PFC converters and PWM rectifiers reviewed above was mainly concerned with the stability of individual converters in the presence of input filters [5], [7], or small-scale (e.g., mobile) power systems with actively regulated loads, such as those found on electric ships [6] and more-electric aircraft [8]. There were scattered efforts (e.g., [9] and [10]) to model power electronic loads for stability study of utility power grids. However, this subject did not gain general attention because practical system stability problems related to power electronic loads in the grid are still rare (with the exception when such loads are highly concentrated, such as in data centers [11] or railway power systems [12]–[14]). The type of load models required for traditional power system stability studies are also relatively simple and developing such models for ac-dc converters did not require a concerted effort by the power electronics community at large.

This changed significantly in recent years due to the rapid development of converter-based generation from renewable sources. Since the best solar and wind resources are usually at remote locations, their development often requires high-voltage dc (HVDC) and other converter-based transmission technologies. As a result, converters are becoming ubiquitous in the power grids, penetrating all aspects of the system, including generation, transmission, and distribution, in addition to traditional applications on the load side. With the plans already announced by many countries and regions to achieve carbon neutrality and 100% renewable by 2050 or sooner, future power systems will undoubtedly be based on converters and be fundamentally different from today's grid. Developing such converter-based power systems will require new modeling and analysis methods at both the converter and the system level as well as new system stability theories and design tools.

From power system point of view, converters are very different from synchronous generators because converters employ much faster control but have very limited ability to withstand overvoltage and overcurrent. The fast control makes a system more dynamic and prone to new stability problems that are uncommon in today's grid. Indeed, new stability problems encountered in recent years in renewable energy and HVDC transmission systems are almost all above the frequency range of traditional power system stability studies, spreading into multiple kilohertz in some cases [15]–[1]. Fundamental-frequency (RMS-value) models that have been used for many decades for traditional power system stability studies cannot capture such high-frequency stability problems; instead, electromagnetic transient (EMT) models that include the fast dynamics of converters must be used. As a result, EMT simulation has become an important tool for the development of renewable energy, HVDC transmission and other converter-based power systems [19].

EMT simulation, however, has several limitations in terms of model availability, fidelity, computation time, and scalability. Numerical simulation is a useful tool for checking/confirming system stability and other transient behavior under specific conditions, but cannot be relied upon for determining system stability in general. It is also difficult to gain insights and develop general solutions to instability problems based solely on numerical simulation. As with existing power system stability theories, frequency-domain analysis based on small-signal models is necessary for practical development. This requires systematic modeling methods and well-characterized frequency-domain models for ac-dc converters that are the fundamental building blocks for power electronics application in the grid.

The dq-frame linearization method reviewed before provides a possible framework to study small-signal dynamics of three-phase ac-dc converters. However, its reliance on a rotating transformation for linearization creates several limitations for practical applications, including difficulties to verify models by measurement, need for the generalized Nyquist criterion because of coupling between d- and q-axis dynamics, and difficulties to handle unbalanced, distorted, asynchronous, or multi-frequency systems [8]. Converters that involve more than one frequency and cannot be linearized in a dq reference frame include modular multilevel converters (MMC) with second-harmonic circulating current control, type-III turbines where the rotor and stator operate at two different frequencies, as well as type-IV turbines when the rectifier and generator dynamics are to be considered at the same time. Since individual converters are modeled in their own dq reference frames, they must be converted to a common reference frame in order to be interconnected to form a system model. The method proposed in the literature to make this conversion requires the voltages at all converter terminals to remain stationary with respect to each other during system transient [20], [21], which is unjustified especially for utility power systems where line impedance plays a central role in system stability and cannot be assumed to cause only a constant voltage angle shift at the fundamental frequency [22].

B. HARMONIC LINEARIZATION

Harmonic linearization is a method to develop small-signal models for ac-dc converters directly in the frequency domain [8]. Compared to linearization in the dq reference frame, harmonic linearization involves no reference frame change, hence the resulting models can be readily connected with each other to form a system model no matter how many converters may be involved. It does not rely on balanced three-phase operation to remove the time-periodic terms, as in the case of dq-frame modeling, hence can be applied to unbalanced (including single phase), distorted, asynchronous, or multi-frequency systems. The general principle of harmonic linearization can be applied to develop small-signal models analytically [23], experimentally based on measurements, or

numerically based on EMT simulation [1], including real-time and control hardware-in-the-loop simulation [25], [26].

One successful application of the method has been in impedance-based stability study of wind, PV and HVDC converters and systems. The impedance-based stability criterion presented in [27] is an extension of the method developed in [1] for dc-dc converters and is applied to three-phase systems based on impedances in different sequences, also referred to as sequence impedances [28]. Harmonic linearization provided a general method to develop small-signal sequence impedance models for this application and has been applied to different types of PV inverters, wind turbines, and HVDC converters, see e.g., [29]. Unlike dq-frame impedances, sequence impedances can be directly measured and, since they are usually uncoupled, are also much easier to understand and use.

Most small-signal sequence impedance models used in the literature have been derived from the basic impedance models of a two-level voltage-source converter (VSC) [23]. Like in the modeling of single-phase PFC converters in [5], the dc bus of the VSC was treated as an ideal voltage source in [23]. The reduced-order models capture the effects of converter current control, phase lock loop (PLL) and control delay, and have been used successfully in the analysis and mitigation of practical renewable energy and HVDC system stability problems related to these control function. However, neglecting dc bus dynamics makes the model inaccurate at low frequencies, especially within 10-30 Hz of the fundamental in which dc bus voltage control has significant effects on converter impedances. The ideal dc bus assumption in effect also neglects any coupling between the ac and dc systems interfaced by the converter, hence will miss an important class of practical system stability problems for which such coupling plays a role, such as stability of HVDC transmission lines connected to weak ac grids, dc microgrids operating in grid-parallel mode, and hybrid ac-dc power systems [30]–[34].

C. MODELING OF AC-DC CONVERTERS AS TWO-PORT NETWORKS

While the procedure used to develop the existing small-signal sequence impedance models can be expanded to include dc bus dynamics for specific applications, as demonstrated in [35], this paper take a more general approach and tackles it in a new framework by modeling a three-phase ac-dc converter as a two-port network, with the three-phase ac terminals treated as one port and the dc terminal as another. The two-port network is characterized in the frequency domain by a set of transfer functions in the form of self and transfer impedance and admittance. Since impedance and admittance share many common properties and are exchangeable, they will be collectively referred to as *immittance*, a term used first in 1945 by Hendrik W. Bode in his classical book [36].

The self and transfer immittances introduced in this work are a generalization of the immittance models of conventional two-port networks, including dc-dc converter Y and H matrix models reviewed at the beginning of this section. The immittance models of ac-dc converters that have been used in the literature correspond to the self immittances of the converter at one port when the other port connects to an ideal voltage source. The transfer immittance models are new and describe two types of coupling that are unique to ac-dc converters:

- *Coupling between ac and dc port*. This manifests in small-signal current responses at one port when the voltage at the other port is perturbed. The different operation frequencies (ac fundamental and dc) of the two ports cause a frequency shift in the current small-signal response when it traverses the converter. Four transfer immittances are defined to model this type of coupling.
- *Coupling over frequency at the ac port*. This manifests in a second ac port current response at frequency $f_p + 2f_1$ or $f_p - 2f_1$ when ac port voltage is perturbed at frequency f_p, f_1 being the fundamental frequency. The frequency shift by $+2f_1$ or $-2f_1$ depends on the sequence of voltage perturbation. Two transfer immittances are defined to model this type of coupling.

The first type of coupling also exists in conventional two-port networks but does not involve a frequency shift and requires only two transfer immittances. The doubled number of transfer immittances required to model this coupling in a three-phase ac-dc converter is due to its three-phase nature, which necessitates a distinction between positive and negative sequence. The second type of coupling does not exist in conventional two-port networks or dc-dc converters. Altogether, the two-port modeling method gives rise to nine small-signal immittance models that fully define small-signal characteristics of a three-phase ac-dc converter at its terminals.

D. SCOPE AND ORGANIZATION OF THE PAPER

The two-port network models defined above can meet the requirements of existing applications reviewed in Subsection I.B as well as new applications that have not been attempted so far. They provide a general framework to characterize small-signal dynamics of ac-dc converters and stability of different power systems (ac, dc, hybrid ac-dc, or asynchronous ac) that involve such converters. The objective of this paper is to present the development and application of the two-port network models. The paper is divided into two parts:

- Part I examines frequency-domain characteristics of ac-dc converters as two-port networks, defines the self and transfer immittances that will be modeled, and presents the development and validation of analytical models.
- Part II [37] shows how the developed models are used to study the stability of different power systems, with an emphasis on renewable energy generation, HVDC transmission, and future hybrid ac-dc grids.

The self and transfer immittances introduced in this paper are general and can be applied to different types of three-phase ac-dc converters, including two-level, multilevel and modular multilevel (MMC) converters. However, to stay focused and be able to present specific models, the work will be limited to two-level voltage-source converters (VSC) that are most widely used in power systems. Multilevel converters and MMC will be treated in a separate paper. The method

applied to develop the immittance models is based on the general principle of harmonic linearization reviewed before. To simplify the algebra and to keep track of multiple frequency components in the linearization process in a more systematic manner, a matrix formulation similar to that presented in [38] for the modeling of MMC will be used.

A preliminary version of the transfer immittance models was presented in [39] for a particular application – to include dc bus dynamics in the output impedance of a grid-connected VSC to improve the accuracy of stability analysis at the converter-grid interface point. The presentation in [39] was brief and did not consider the broad application that this paper aims at. Given the general applicability of the modeling method and the resulting models, development in this paper will be presented in much greater detail to serve also as a tutorial on frequency-domain modeling and stability analysis of ac-dc converters and systems in general.

The rest of Part I is organized as follows: Section II defines the circuit and control of the two-level VSC that will be modeled in this work, explains its representation as a two-port network, and identifies the coupling phenomena in the converter's frequency-domain responses. Section III formally defines the immittance models to be developed and reviews the general modeling method based on multi-harmonic linearization. Section IV presents step-by-step development of the defined immittance models, giving each model in an analytical form at the end. Sequence relationship will also be presented to reduce the number of independent models. Section V presents validation of the developed analytical models, possible ways to simplify them, and important characteristics revealed by the models. Section VI concludes Part I of the work.

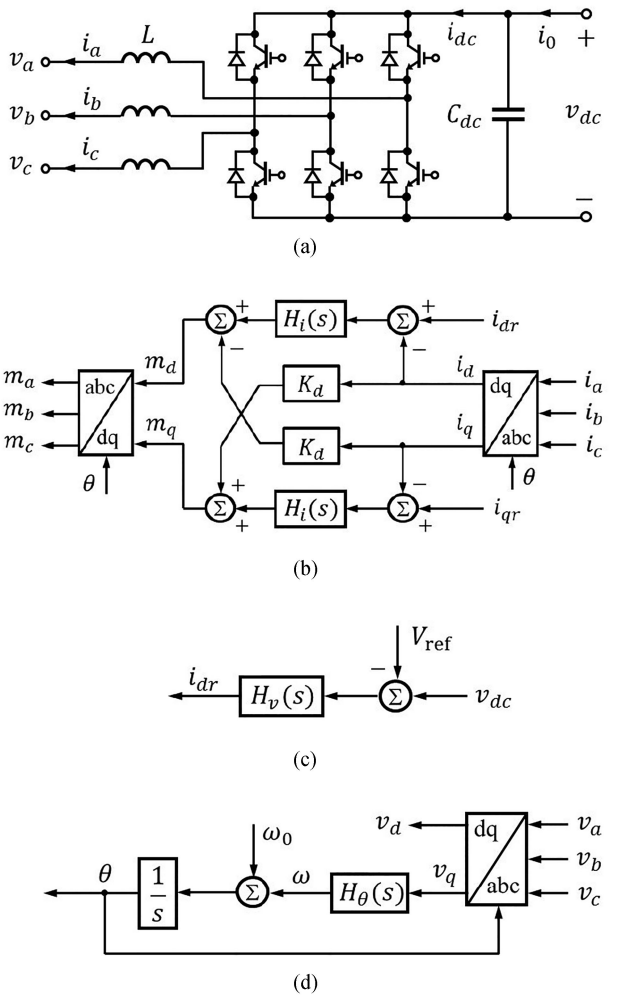

FIGURE 1. Circuit and control of the two-level three-phase ac-dc converter modeled in this work: (a) converter circuit; (b) ac-port current control in dq frame; (c) dc bus voltage control; and d) phase-locked loop (PLL).

II. AC-DC CONVERTERS AS TWO-PORT NETWORKS

Fig. 1(a) shows the principal circuit of the two-level ac-dc converter that will be modeled in this work. The converter is a common building block for many grid-related applications, including type-III and type-IV turbines, PV inverters, STATCOM, energy storage and HVDC transmission.

Control of the converter is illustrated in Fig. 1(b)–(d) and includes three-phase current control (Fig. 1(b)), dc bus voltage control (Fig. 1(c)), and synchronization to the ac voltage by a phase lock loop (PLL, Fig. 1(d)). Ac current control is assumed to be performed in the dq reference frame, which is common in grid applications.

A. CONVERTER MODELS AND LINEARIZATION

Based on the notations introduced in Fig. 1(a)), dynamics of the converter power stage are described by the following switching-cycle averaged model, where d_x $(x = a,\ b,\ c)$ denote the duty ratio of the upper switch in each phase and v_m is the voltage of the middle of the dc bus (relative to the same neutral reference point to which the phase voltages v_a, v_b and v_c are measured):

$$L\frac{d}{dt}\begin{bmatrix} i_a \\ i_b \\ i_c \end{bmatrix} = \begin{bmatrix} d_a \\ d_b \\ d_c \end{bmatrix} v_{dc} - \begin{bmatrix} v_a \\ v_b \\ v_c \end{bmatrix} - \left\{ \frac{1}{2}\begin{bmatrix} v_{dc} \\ v_{dc} \\ v_{dc} \end{bmatrix} - \begin{bmatrix} v_m \\ v_m \\ v_m \end{bmatrix} \right\} \tag{1}$$

$$C\frac{dv_{dc}}{dt} = i_0 - (d_a i_a + d_b i_b + d_c i_c) \tag{2}$$

The terms inside the curly brackets in (1) are the same among the three phases. Each represents the common-mode voltage of the converter and will be denoted as v_{cm} in the following development. This voltage does not cause a current response at the ac terminal and will eventually be eliminated.

Each equation in (1) includes a nonlinear (bilinear) term involving the duty ratio and dc bus voltage. Similar nonlinearity exists in the dc bus voltage model (2). Control of the converter is usually linear, but the transformation between the phase (abc) and the dq frame introduces another nonlinear function, which is also part of the PLL and is defined as follows in this

work:

$$\begin{bmatrix} x_d \\ x_q \end{bmatrix} = \mathbf{T}_{dq}(\theta) \begin{bmatrix} x_a \\ x_b \\ x_c \end{bmatrix} \tag{3}$$

$$\mathbf{T}_{dq}(\theta) = \sqrt{\frac{2}{3}} \begin{bmatrix} \cos\theta & \cos\left(\theta - \frac{2\pi}{3}\right) & \cos\left(\theta + \frac{2\pi}{3}\right) \\ -\sin\theta & -\sin\left(\theta - \frac{2\pi}{3}\right) & -\sin\left(\theta + \frac{2\pi}{3}\right) \end{bmatrix}$$

Each of these nonlinear terms must be linearized when developing small-signal models for the converter. To reduce complexity, the dc bus voltage was assumed constant in the development of the small-signal sequence impedance models presented in [23]. This assumption rendered (1) linear and (2) unnecessary, such that only control nonlinearity has to be dealt with. The resulting positive- and negative-sequence impedance models are accurate above the second harmonic frequency ($2f_1$) in general. In conjunction with the impedance-based stability criterion presented in [27], these models provided a practical method for the modeling and mitigation of new stability and resonance problems in renewable energy and HVDC systems.

Most problems considered in the early work on impedance-based stability modeling and analyses were in the "harmonic frequency" range for which the basic sequence impedance models presented in [23] were adequate. The basic models also captured the negative damping effects introduced by the PLL, hence can be used to analyze PLL-related resonance and instability problems, which are typically below or near the fundamental frequency. For example, the models were used to characterize and solve subsynchronous resonance (SSR) of type-III turbines with series-compensated overhead transmission lines in [1]–[42] and of type-IV turbines and PV inverters with weak grids in [43]–[44]. However, as the interests in SSR and other low-frequency stability problems grew, it also became apparent that small-signal models incorporating the dc bus dynamics are required.

The modeling procedure used in [23] can be expanded to include dc bus dynamics, which was the approach taken in [35]. However, the resulting models are highly complex and implicit because they have to be solved from a set of matrix equations. The difficulty is partly caused by the control-oriented approach adopted in [35] in which perturbation is applied at the ac and dc terminal of the converter simultaneously to linearize the entire model at once. The resulting models are complete but virtually impossible to work with analytically. To overcome this difficulty, we present here a network-oriented approach, which treats the converter as a two-port network and linearizes it as such by applying a voltage perturbation at one port at a time. The approach is similar to that used in [2] to characterize dc-dc converters.

B. DEFINITION OF TWO-PORT NETWORK

To represent and model the VSC of Fig. 1 as a two-port network, we have to define the two-port network first. There are several options for this definition. Our goal is to define it such that the resulting two-port models are as generally applicable as possible while keeping them simple and their development mathematically trackable.

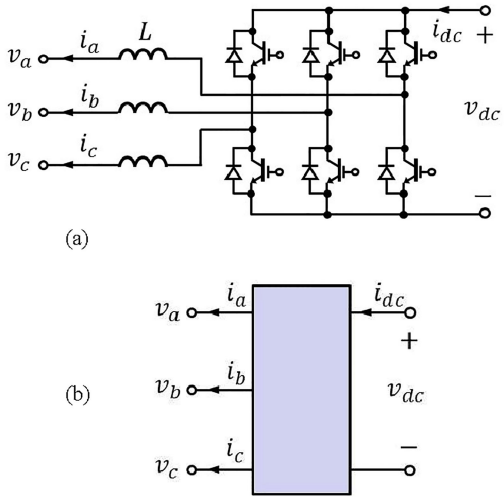

FIGURE 2. Two-level voltage-source converter (a) and its representation as a two-port network (b).

At the ac terminal, the three inductors and their current control are an integral part of any three-phase VSC. Excluding these inductors would require the two-port network to interface with current sources at the ac terminal, which has to be characterized differently. The dc capacitor is also a necessary part of a VSC, but it may be shared by two or more converters, such as in the case of two VSCs connected back-to-back. If the dc capacitor were considered part of the two-port network, one would have to decide how to split the dc bus capacitance between two or more converters that share a common dc bus, which adds unnecessary ambiguity and complication. Including the dc capacitor as part of the two-port network also increases the order of the converter circuit model, adding more complexity to the development as well as the final results. On the other hand, the dc capacitor is a linear component by itself and can be easily added to the two-port network model after linearization.

Based on these considerations, we define the two-port network to include three ac phase inductors but exclude the dc bus capacitor, as illustrated in Fig. 2. All three control functions defined in Fig. 1 are also included, although they are not explicitly shown in Fig. 2.

Compared to dc-dc converters or conventional two-port networks, the two-port network defined here has three phases at its ac port. An alternative might be to treat each phase as a separate port and model the converter as a multiport network. However, since the three phases are always controlled and operated together, it makes no sense to treat them as independent ports. On the other hand, the added degree of freedom at the ac port necessitates a generalization to the existing two-port network theory and characterization method. The three phase currents are also dependent of each other, hence cannot all be used as port variables.

The technique we apply to deal with these complexities is based on the symmetrical component theory, which represents a set of three-phase variables by decomposing each into a positive-sequence, a negative-sequence, and a zero-sequence component. The components in each sequence are balanced among the three phases and follow a specific sequence. Application of the symmetrical component theory had been limited to steady-state (fundamental) fault current calculation in traditional power systems, but the method, defined by the complex transformation matrix $\mathbf{S}$ given below, is applicable to three-phase variables at any frequency.

$$\mathbf{S} = \frac{1}{3}\begin{bmatrix} 1 & 1 & 1 \\ 1 & \mathbf{a} & \mathbf{a}^2 \\ 1 & \mathbf{a}^2 & \mathbf{a} \end{bmatrix}, \ \mathbf{a} = e^{j\frac{2\pi}{3}} \tag{4}$$

To characterize the two-port network defined in Fig. 2 in the frequency domain, we apply a voltage perturbation at certain frequency to one of the ports and find the current responses at both ports. Since the ac port has three phases, the perturbation has to be of three phase as well. Denoting the frequency of perturbation as f_p, we can write the perturbed three-phase voltages as follows where V_1 is the fundamental voltage amplitude, f_1 is the fundamental frequency, $\omega_1 = 2\pi f_1$, $\omega_p = 2\pi f_p$, and the magnitude of perturbation $\{\Delta V_a, \Delta V_b, \Delta V_c\}$ should be much smaller than V_1:

$$\begin{bmatrix} v_a \\ v_b \\ v_c \end{bmatrix} = V_1 \begin{bmatrix} \cos(\omega_1 t) \\ \cos\left(\omega_1 t - \frac{2\pi}{3}\right) \\ \cos\left(\omega_1 t - \frac{4\pi}{3}\right) \end{bmatrix} + \begin{bmatrix} \Delta V_a \cos(\omega_p t + \varphi_a) \\ \Delta V_b \cos(\omega_p t + \varphi_b) \\ \Delta V_c \cos(\omega_p t + \varphi_c) \end{bmatrix} \tag{5}$$

Note that the fundamental components are balanced and in the positive sequence. This assumption will be made for all steady-state operations of the converter. The three small-signal perturbations are at the same frequency but have different amplitudes and their initial phase angles are not necessarily symmetrical; in other words, they are unbalanced in general. This is necessary for keeping the perturbations independent among the three phases so as to avoid perturbing the converter in a particular manner that may limit the usefulness of the resulting models. However, unbalanced three-phase signals are difficult to work with. To simplify the problem, we first express the unbalanced three-phase perturbations by a set of symmetrical components by applying the symmetrical component transformation (4) to (5):

$$\begin{bmatrix} \Delta V_a \cos(\omega_p t + \varphi_a) \\ \Delta V_b \cos(\omega_p t + \varphi_b) \\ \Delta V_c \cos(\omega_p t + \varphi_c) \end{bmatrix} = \Delta V_p \begin{bmatrix} \cos(\omega_p t + \varphi_p) \\ \cos\left(\omega_p t + \varphi_p - \frac{2\pi}{3}\right) \\ \cos\left(\omega_p t + \varphi_p - \frac{4\pi}{3}\right) \end{bmatrix} + \Delta V_n \begin{bmatrix} \cos(\omega_p t + \varphi_n) \\ \cos\left(\omega_p t + \varphi_n - \frac{4\pi}{3}\right) \\ \cos\left(\omega_p t + \varphi_n - \frac{2\pi}{3}\right) \end{bmatrix} + \Delta V_0 \begin{bmatrix} \cos(\omega_p t + \varphi_0) \\ \cos(\omega_p t + \varphi_0) \\ \cos(\omega_p t + \varphi_0) \end{bmatrix} \tag{6}$$

This relationship indicates that, instead of three-phase perturbations with independent amplitudes and phases, characterization of the defined two-port network at the ac port may use a linear combination of balanced three-phase perturbations in the positive, negative and zero sequence. Based on (6), these sequence components should be applied all at once. However, this can be further simplified based on the following considerations:

- Without a neutral connection, the converter does not respond to voltages in the zero sequence; hence the zero-sequence components in (6) can be excluded, such that only positive- and negative-sequence perturbations are needed.
- The converter response to small-signal perturbation should be linear. Therefore, the response to a combined positive- and negative-sequence perturbation can be obtained by separately applying a perturbation in one sequence at a time and combining the responses afterwards.
- Since small-signal response should be time-invariant and independent of the time at which the perturbation is injected, the initial phase angles $\{\varphi_p, \varphi_n\}$ in (6) can be set to zero to simplify the notation further.

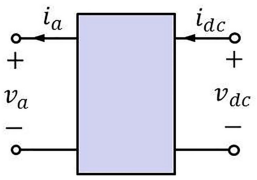

FIGURE 3. Two-port network representation of a three-phase VSC for mathematical modeling based on symmetrical components.

Accordingly, small-signal characterization of the defined two-port network at its ac port can be performed by applying the following voltage perturbations one at a time:

- Positive Sequence:

$$\begin{bmatrix} \hat{v}_a \\ \hat{v}_b \\ \hat{v}_c \end{bmatrix} = \Delta V_p \begin{bmatrix} \cos \omega_p t \\ \cos\left(\omega_p t - \frac{2\pi}{3}\right) \\ \cos\left(\omega_p t - \frac{4\pi}{3}\right) \end{bmatrix} \tag{7}$$

- Negative Sequence:

$$\begin{bmatrix} \hat{v}_a \\ \hat{v}_b \\ \hat{v}_c \end{bmatrix} = \Delta V_n \begin{bmatrix} \cos \omega_p t \\ \cos\left(\omega_p t - \frac{4\pi}{3}\right) \\ \cos\left(\omega_p t - \frac{2\pi}{3}\right) \end{bmatrix} \tag{8}$$

Note that a set of balanced three-phase perturbation is fully defined when its sequence and phase-a component are specified. For instance, (7) is defined when we specify it as a positive sequence with $\Delta V_p \cos \omega_p t$ as the phase-a voltage. Therefore, for the purpose of mathematical development, phase b and c are redundant and can be removed from the two-port network defined in Fig. 2, with the understanding that any variable of the remaining phase-a terminal actually represents a symmetrical component among three phases. This leads to a semantically "true" two-port network depicted in Fig. 3, with phase a as one port and the dc terminal as the second port.

C. TRANSFER CHARACTERISTICS

In conventional network theory, a two-port network is characterized by an 2×2 immittance matrix. Each diagonal element

of the matrix defines the response of a port current to the voltage applied at the same port. Off-diagonal elements describe the transfer (or transmission) between the two ports and are referred to as a transfer immittance in this work. When the network is nonlinear, a linearized model is developed based on small-signal responses at each port of the network. This was how the admittance (Y) matrix model was developed in [2] for dc-dc converters.

The method to characterize the two-port network defined above for ac-dc converters follows the same principle but is different in several aspects. First, because of the presence of variables at the fundamental frequency, linearization must be performed in the frequency domain by assuming a sinusoidal perturbation (harmonic linearization) instead of an arbitrary function of time. Secondly, unlike in a dc-dc converter or any network operating with dc at both ports, there is a frequency shift between the ac and dc port of an ac-dc converter. This frequency shift also appears in the converter's small-signal response and requires the transfer immittances to be defined differently. Thirdly, the two-port network has to be characterized by a positive-sequence as well as a negative-sequence perturbation at the ac port, which implies more transfer functions have to be developed. The general principle of harmonic linearization has been reviewed in Subsection I.B and will be further discussed in the next section. In the following, we will address the remaining two aspects in order to understand the behavior that will be modeled by transfer immittances.

To see how frequency shifts when a perturbation traverses an ac-dc converter, assume first that the converter operates in a steady state with balanced (positive-sequence) currents at the fundamental frequency f_1, as specified below where the symbol "$\propto$" means "is proportional to":

$$\begin{bmatrix} i_a \\ i_b \\ i_c \end{bmatrix} \propto \begin{bmatrix} \cos \omega_1 t \\ \cos\left(\omega_1 t - \frac{2\pi}{3}\right) \\ \cos\left(\omega_1 t - \frac{4\pi}{3}\right) \end{bmatrix} \tag{9}$$

Consider now that a positive-sequence voltage perturbation at frequency f_p, as defined by equation (7), is applied at the ac port. Through interaction with the steady-state currents specified by (9), this voltage perturbation causes a variation in the power flowing out of the ac port:

$$\begin{aligned} \Delta p \propto \sum_{k=0}^{2} \cos\left(\omega_p t - \tfrac{2k\pi}{3}\right) \cdot \cos\left(\omega_1 t - \tfrac{2k\pi}{3}\right) = \\ \tfrac{3}{2}\cos\left[\left(\omega_p - \omega_1\right) t\right] + \tfrac{1}{2}\sum_{k=0}^{2} \cos\left[\left(\omega_p + \omega_1\right) t - \tfrac{4k\pi}{3}\right] \end{aligned} \tag{10}$$

Note that the terms at frequency $\omega_p + \omega_1$ on the right-hand side of (10) are symmetrical and add to zero, leaving only the term at frequency $\omega_p - \omega_1$. Under lossless operation assumption of the converter, the power defined by (10) has to be balanced by a similar variation in the dc-port power, which implies a current at frequency $f_p - f_1$ into the dc port. Therefore, the transfer admittance defining the relationship from a positive-sequence perturbation in the ac-port voltage to the dc-port current response has to include a downshift of frequency by f_1. Similarly, it can be shown that the transfer admittance defining the relationship from a negative-sequence perturbation in the ac-port voltage to the dc-port current response has to include an upshift of frequency by f_1.

There is a similar shift in frequency in the ac-port current response to a dc-port voltage perturbation. To see that, note that the duty ratios of the converter in steady state are balanced (positive sequence) and vary at the fundamental frequency. Without losing generality, ignore the possible phase difference between the duty ratio and the phase current (9), such that the three duty ratio signals can be expressed as follows:

$$\begin{bmatrix} d_a \\ d_b \\ d_c \end{bmatrix} \propto \begin{bmatrix} \cos \omega_1 t \\ \cos\left(\omega_1 t - \frac{2\pi}{3}\right) \\ \cos\left(\omega_1 t - \frac{4\pi}{3}\right) \end{bmatrix} \tag{11}$$

Assume now that a perturbation at frequency f_p is added to the dc-port voltage. This voltage perturbation will also be modulated by the steady-state duty ratios (11), causing a perturbation at two different frequencies ($\omega_p \pm \omega_1$) in each phase of the converter ac-terminal voltages:

$$\begin{aligned} \cos \omega_p t \begin{bmatrix} \cos \omega_1 t \\ \cos\left(\omega_1 t - \frac{2\pi}{3}\right) \\ \cos\left(\omega_1 t - \frac{4\pi}{3}\right) \end{bmatrix} &= \frac{1}{2}\begin{bmatrix} \cos\left(\omega_p - \omega_1\right) t \\ \cos\left(\left(\omega_p - \omega_1\right) t - \frac{4\pi}{3}\right) \\ \cos\left(\left(\omega_p - \omega_1\right) t - \frac{2\pi}{3}\right) \end{bmatrix} \\ &+ \frac{1}{2}\begin{bmatrix} \cos\left(\omega_p + \omega_1\right) t \\ \cos\left(\left(\omega_p + \omega_1\right) t - \frac{2\pi}{3}\right) \\ \cos\left(\left(\omega_p + \omega_1\right) t - \frac{4\pi}{3}\right) \end{bmatrix} \end{aligned} \tag{12}$$

The resulting ac-terminal voltage perturbation at each frequency will in turn cause a response in the phase current at the same frequency. Therefore, two transfer admittances are required to describe the transfer from dc-port voltage to ac-port current, each of which involves a shift in frequency either up or down by the fundamental. Note also from (12) that the responses at $f_p + f_1$ form a positive sequence while the ones at $f_p - f_1$ form a negative sequence.

The frequency shift phenomena explained above can be traced back to the bilinear terms involving duty ratios in the converter models (1)–(2). They correspond to the first type of coupling discussed in Subsection I.B.

The bilinear terms are also responsible for the second type of coupling that requires additional transfer immittance models. To explain that, recall from (10) that a positive-sequence voltage perturbation at f_p causes the dc-port current to vary at frequency $f_p - f_1$. Through impedance of the dc bus capacitor, this current produces a perturbation in the dc-port voltage at the same frequency, which, when modulated by the steady-state duty ratios (11), leads to two frequency components in

the phase voltages (hence also phase currents):

$$\cos\left(\omega_p-\omega_1\right)t\begin{bmatrix}\cos\omega_1 t\\ \cos\left(\omega_1 t-\frac{2\pi}{3}\right)\\ \cos\left(\omega_1 t-\frac{4\pi}{3}\right)\end{bmatrix}=\frac{1}{2}\begin{bmatrix}\cos\omega_p t\\ \cos\left(\omega_p t-\frac{2\pi}{3}\right)\\ \cos\left(\omega_p t-\frac{4\pi}{3}\right)\end{bmatrix}+\frac{1}{2}\begin{bmatrix}\cos\left(\omega_p-2\omega_1\right)t\\ \cos\left(\left(\omega_p-2\omega_1\right)t-\frac{4\pi}{3}\right)\\ \cos\left(\left(\omega_p-2\omega_1\right)t-\frac{2\pi}{3}\right)\end{bmatrix}\tag{13}$$

The first term on the right-hand side of (13) are at the same frequency and in the same (positive) sequence as the original voltage perturbation; it is modeled by the self admittance of the ac port. The second term, at frequency f_p-2f_1, is in the negative sequence and represents an additional component in the ac-port current that is not modeled by any of the admittance or transfer admittance discussed so far.

A similar coupling occurs in the response to a negative-sequence voltage perturbation. However, since the frequency of the dc-port current is f_p+f_1 when a negative-sequence voltage perturbation at f_p is applied, this second current response will be at frequency f_p+2f_1 and is in the positive sequence, as can be seen from the following expansion:

$$\cos\left(\omega_p+\omega_1\right)t\begin{bmatrix}\cos\omega_1 t\\ \cos\left(\omega_1 t-\frac{2\pi}{3}\right)\\ \cos\left(\omega_1 t-\frac{4\pi}{3}\right)\end{bmatrix}=\frac{1}{2}\begin{bmatrix}\cos\omega_p t\\ \cos\left(\omega_p t-\frac{4\pi}{3}\right)\\ \cos\left(\omega_p t-\frac{2\pi}{3}\right)\end{bmatrix}+\frac{1}{2}\begin{bmatrix}\cos\left(\omega_p+2\omega_1\right)t\\ \cos\left(\left(\omega_p+2\omega_1\right)t-\frac{2\pi}{3}\right)\\ \cos\left(\left(\omega_p+2\omega_1\right)t-\frac{4\pi}{3}\right)\end{bmatrix}\tag{14}$$

III. IMMITTANCE MODELS AND MODELING METHOD

This section defines the immittances that will be modeled, discusses the completeness of these models, and explains the method to develop the models.

A. MATHEMATICAL DEFINITION

It can be concluded from last section that an ac-dc converter as a two-port network can be characterized by applying a voltage perturbation to one of the ports at a time and modeling the resulting current responses at both ports. Perturbation at the ac port should use positive and negative sequences. With each perturbation, the current of the same port at the same frequency defines the self immittance of that port, while the current of the other port or of the same port but at another frequency defines a transfer immittance.

For the purpose of mathematical development, we will denote the small-signal component of a variable at certain frequency by a "hat" above the variable and the frequency in parentheses next to it. For example, $\hat{v}_{dc}(f_p)$ denotes the small-signal component at frequency f_p in the dc bus voltage v_{dc}. To shorten the expression, angular frequency will be used in place of ordinary frequency whenever convenient and be denoted by symbol ω with the same subscript, for instances, $\omega_1=2\pi f_1$, $\omega_p=2\pi f_p$ and $\omega=2\pi f$. In the final models, the complex frequency s will also be used in place of $j\omega_p$. For instance, $\hat{i}_a(f_p+f_1)$ may be written as $\hat{i}_a(j\omega_p+j\omega_1)$ or $\hat{i}_a(s+j\omega_1)$. Since we are working with multiple frequencies, the following frequency variables will also be used to shorten the expressions whenever appropriate:

$$\begin{cases}f_{p-1}\triangleq f_p-f_1\\ f_{p+1}\triangleq f_p+f_1\\ f_{p-2}\triangleq f_p-2f_1\\ f_{p+2}\triangleq f_p+2f_1\end{cases}$$

$$\begin{cases}\omega_{p-1}\triangleq \omega_p-j\omega_1\\ \omega_{p+1}\triangleq \omega_p+j\omega_1\\ \omega_{p-2}\triangleq \omega_p-j2\omega_1\\ \omega_{p+2}\triangleq \omega_p+j2\omega_1\end{cases}$$

$$\begin{cases}s_{-1}\triangleq s-j\omega_1\\ s_{+1}\triangleq s+j\omega_1\\ s_{-2}\triangleq s-j2\omega_1\\ s_{+2}\triangleq s+j2\omega_1\end{cases}$$

Each self and transfer immittance will be denoted by double subscripts using three letters $\{p,\ n,\ d\}$ that specify the port and sequence of variables involved in the definition: p for positive sequence at the ac port, n for negative sequence at the ac port, and d for the dc port. The first subscript indicates the port at which the voltage perturbation is applied and its sequence (if it is at the ac port). The second subscript indicates the port (and sequence) of the current response that the transfer function measures. For example, Y_{pd} denotes the transfer admittance from a positive-sequence voltage perturbation at the ac port to the current response at the dc port. For transfer immittances, the notation does not indicate the frequency shift between the voltage perturbation and the current response; this aspect is embedded in the definition and can be inferred from the principle of coupling discussed before.

Using these nomenclatures, Table I gives the mathematical definition of the immittance models describing the two-port network. The negative signs in front of the transfer functions defined by a voltage perturbation at the ac port are included to account for the particular current reference direction given in Figs. 1 and 3 and to make the definitions consistent with that of conventional two-port networks. The nine transfer functions are all defined as admittances but can also be expressed as impedances. They are divided into three groups, each as the result of a voltage perturbation at the ac or dc port:

- With a positive-sequence voltage perturbation $\hat{v}_p(f_p)$ at the ac port, the converter responds with a) a positive-sequence current at frequency f_p at the ac port, which defines the positive-sequence admittance $Y_{pp}(s)$ of the ac port; b) a current at frequency f_p-f_1 at the dc port, which defines a transfer admittance of the first type and is denoted as $Y_{pd}(s)$; and c) a negative-sequence current at frequency f_p-2f_1 at the ac port, which defines a transfer admittance of the second type and is denoted as $Y_{pn}(s)$.

TABLE I. Mathematical Definition of Immittance Models

Voltage Perturbation	Self Admittance	Transfer Admittance	
AC Port, Positive Sequence $\hat{v}_p(s)$	$Y_{pp}(s) = -\dfrac{\hat{\imath}_a(s)}{\hat{v}_p(s)}$	$Y_{pd}(s) = -\dfrac{\hat{\imath}_{dc}(s-j\omega_1)}{\hat{v}_p(s)}$	$Y_{pn}(s) = -\dfrac{\hat{\imath}_a(s-j2\omega_1)}{\hat{v}_p(s)}$
AC Port, Negative Sequence $\hat{v}_n(s)$	$Y_{nn}(s) = -\dfrac{\hat{\imath}_a(s)}{\hat{v}_n(s)}$	$Y_{nd}(s) = -\dfrac{\hat{\imath}_{dc}(s+j\omega_1)}{\hat{v}_n(s)}$	$Y_{np}(s) = -\dfrac{\hat{\imath}_a(s+j2\omega_1)}{\hat{v}_n(s)}$
DC Port $\hat{v}_{dc}(s)$	$Y_{dd}(s) = \dfrac{\hat{\imath}_{dc}(s)}{\hat{v}_{dc}(s)}$	$Y_{dp}(s) = \dfrac{\hat{\imath}_a(s+j\omega_1)}{\hat{v}_{dc}(s)}$	$Y_{dn}(s) = \dfrac{\hat{\imath}_a(s-j\omega_1)}{\hat{v}_{dc}(s)}$

- With a negative-sequence voltage perturbation $\hat{v}_n(f_p)$ at the ac port, the converter responds with a) a negative-sequence current at frequency f_p at the ac port, which defines the negative-sequence admittance $Y_{nn}(s)$ of the ac port; b) a current at frequency $f_p + f_1$ at the dc port, which defines a transfer admittance of the first type and is denoted as $Y_{nd}(s)$; and c) a positive-sequence current at frequency $f_p + 2f_1$ at the ac port, which defines a transfer admittance of the second type and is denoted as $Y_{np}(s)$.
- With a voltage perturbation $\hat{v}_{dc}(f_p)$ at the dc port, the converter responds with a) a current at frequency f_p at the dc port, which defines the self admittance $Y_{dd}(s)$ of the dc port; b) a positive-sequence current at frequency $f_p + f_1$ and a negative-sequence current at frequency $f_p - f_1$ at the ac port, which define the last two transfer admittances denoted as $Y_{dp}(s)$ and $Y_{dn}(s)$, respectively.

The positive- and negative-sequence impedance models developed in [23] correspond to the self admittances Y_{pp} and Y_{nn} defined in Table I. The dc-port self admittance Y_{dd} has been modeled in the literature for HVDC system stability analysis and is usually developed by linearization of the converter model in the dq frame or by assuming ideal current control [45]. The coupled ac-port current response at frequency $f_p \pm 2f_1$ caused by PLL nonlinearity was discussed in [46]. The transfer admittances Y_{pn} and Y_{np} defined in this work provide a more general framework to describe this phenomenon and makes it possible to include not only the PLL but also dc bus dynamics and other types of nonlinearity. The remaining four transfer admittances, namely, Y_{pd}, $Y_{nd}(s)$, $Y_{dp}(s)$ and $Y_{dn}(s)$, describe small-signal coupling between the ac and dc port that have not been considered in the literature but are important for a number of existing and emerging applications, as discussed in Section I and will be presented in Part II of the paper.

B. COMPLETENESS OF THE DEFINED MODELS

As pointed out before, the frequency shift in each of the transfer admittances is due to the nonlinearity in the converter and control model. Since the nonlinearity acts on all frequency components continuously, one might ask if this may lead to a chain of reaction and create responses at more frequencies besides $f_p \pm f_1$ and $f_p \pm 2f_1$, thereby necessitating the use of more transfer immittances. More generally, could there be currents at frequency $mf_p \pm nf_1$ (with $m > 1$ and $n > 2$) that also have to be included as part of the small-signal model?

To answer this question, recall first that small-signal analysis is about responses that are linearly proportional to the perturbation. With a perturbation at frequency f_p, generation of a small-signal response at frequency $2f_p \pm nf_1$ would require the "interaction" (e.g., multiplication) of two small-signal variables at f_p. Since the amplitude of each small-signal variable is supposed to be proportional to the perturbation, the product of two such signals is a higher-order term of the perturbation, hence can be neglected in small-signal modeling. Therefore, we only need to consider responses at frequency $f_p \pm nf_1$ in small-signal analysis.

To see if small-signal responses at $f_p \pm nf_1$ with $n > 2$ may exist, recall from the discussion in Subsection II.C that a shift in frequency by $\pm f_1$ is created when a small-signal variable is multiplied with a steady-state variable at the fundamental frequency. (Since such multiplication involves only one small-signal variable, the result is linearly proportional to the perturbation, hence would have to be included in small-signal modeling.) Consider as an example the second current response at $f_p - 2f_1$ produced by a positive-sequence voltage perturbation at the ac port. Like a perturbation at f_p, this current also interacts with the fundamental voltage and causes the dc-port power (hence also the current) to vary. Since the current at $f_p - 2f_1$ is in negative sequence, the frequency of the resulting dc-port current variation is the upshift of $f_p - 2f_1$ by f_1, which is the same as the frequency of the dc-port current induced by the original positive-sequence perturbation at f_p:

$$(f_p - 2f_1) + f_1 = f_p - f_1$$

Therefore, $\{f_p,\ f_p - f_1,\ f_p - 2f_1\}$ represent the frequencies of all possible small-signal responses when a positive-sequence voltage perturbation is applied to the ac-port. This closed "chain of reaction" is illustrated in Fig. 4(a). Similarly, it can be shown that $\{f_p,\ f_p + f_1,\ f_p + 2f_1\}$ are all the small-signal components produced by a negative-sequence voltage perturbation at the ac-port, and $\{f_p,\ f_p + f_1,\ f_p - f_1\}$ represent all small-signal components that a dc-port voltage perturbation may generate, as illustrated in Fig. 4(b) and 4(c), respectively. Therefore, the three self admittances and six

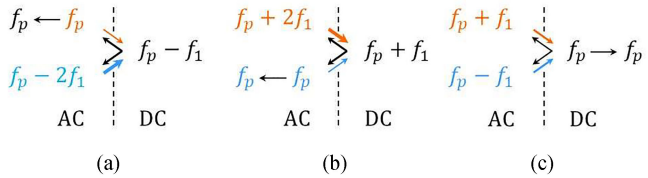

FIGURE 4. Frequencies of small-signal responses induced by a voltage perturbation at frequency f_p at (a) ac port in positive sequence, (b) ac port in negative sequence, and (c) dc port.

transfer admittances defined in Table I form a complete set of small-signal models for a three-phase ac-dc converter.

The closed "chain of reaction" explained above is unique to three-phase ac-dc converters. It does not hold when the operation is unbalanced or in single-phase converters – in each case a small-signal perturbation at f_p at either the ac or dc port may produce current responses at infinite number of frequencies $f_p \pm nf_1, n = 0,\ 1,\ 2,\ \ldots,\ \infty$. The development of low-frequency input impedance models for single-phase PFC converters in [11] considered this more complex behavior.

The coupled current responses modeled by Y_{pn} and Y_{np} have generated considerable discussions in the last few years. A number of papers promulgated this as a proof for the need to couple positive and negative sequence models in a matrix form, see e.g., [21] and [46]. Several papers also claimed "generalized" or "unified" impedance modeling and system stability analysis methods based on such characterization. However, this is a misinterpretation of the relationship and responses modeled by Y_{pn} and Y_{np}. Subsection V.B will address this topic in more detail.

It is also worth noting that complete characterization of a three-phase ac-dc converter in the dq reference frame would require independent perturbation at the dc terminal as well as in both d and q axis at the ac terminal, which also leads to nine transfer functions. However, unlike the sequence immittances defined in Table I, dynamics of a converter in the d- and q-axis are coupled in general and have to be used together [8]. This is an important advantage of the sequence immittance models. A mathematic relationship between positive- and negative-sequence responses will also be presented in the next section that will allow models of $\{Y_{nn},\ Y_{nd},\ Y_{np}\}$ to be mathematically related to $\{Y_{pp},\ Y_{pd},\ Y_{pn}\}$, bringing down the total number of "independent" transfer functions from nine to six.

C. MODELING BY MULTI-HARMONIC LINEARIZATION

Development of the self and transfer admittance models defined in Table I will be presented in the next section. The modeling method, based on harmonic linearization, involves introducing a small sinusoidal voltage perturbation to each port and calculating the resulting current responses at different frequencies. Since the objective is frequency-domain models, the mathematical development is also performed in the frequency domain by representing each variable as a Fourier series. Each nonlinear term in the model is expanded algebraically. The terms at the same frequency in each model are then collected together, and the principle of harmonic balance is invoked to formulate an algebraic equation involving the Fourier coefficients of different variables at the same frequency. The equations are then solved to define each of the required current responses.

The positive- and negative-sequence impedance models presented in [23] were developed by directly applying the method outlined above. The algebraic manipulation involved in the derivation was tedious but manageable. With the addition of dc bus dynamics and the inclusion of new frequency components at $f_p \pm f_1$ and $f_p \pm 2f_1$, the number of small-signal terms that have to be considered increases drastically and becomes very difficult to track individually. The matrix-based formulation presented in [38] overcomes this difficulty and will be used in this work. To prepare for the development in the next section, we review the method here and introduce the notations that will be used.

To explain the method, consider the phase-a current model, which is part of (1) and is reproduced below:

$$L\frac{di_a}{dt} = d_a v_{dc} - v_a - v_{cm} \tag{15}$$

The common-mode voltage v_{cm} is dependent of other variables and will be removed in the final model. Here we treat it as an independent variable. To linearize (15), assume each variable in it consists of a steady-state and a small-signal component. Denoting the (periodic) steady-state component by "$\sim$" over the variable and the small-signal component by a hat "^", as introduced before, we can change (15) into

$$L\frac{d\left(\tilde{i}_a + \hat{i}_a\right)}{dt} = \left(\tilde{d}_a + \hat{d}_a\right)\left(V_{dc} + \hat{v}_{dc}\right) - \left(\tilde{v}_a + \hat{v}_a\right) - \left(\tilde{v}_{cm} + \hat{v}_{cm}\right)$$

From this equation, the following model is obtained for the small-signal components:

$$L\frac{d\hat{i}_a}{dt} = \tilde{d}_a\hat{v}_{dc} + V_{dc}\hat{d}_a - \hat{v}_a - \hat{v}_{cm} \tag{16}$$

This is a time-periodic model and cannot be converted to the frequency domain by Laplace transformation because the coefficient of $\hat{v}_{dc}$ on the right-hand side varies at the fundamental frequency. The root cause for this time-periodic term is the bilinear term between d_a and v_{dc} in (15), which is a common form of nonlinearity in ac-dc converter models. Harmonic linearization overcomes this difficulty by carrying out the linearization in the frequency-domain directly. To make the formulation and notations more general, consider first a generic bilinear function $z(t) = x(t)y(t)$ where $x(t)$ and $y(t)$ each consists of a steady state and a small-signal component:

$$x(t) = \tilde{x}(t) + \hat{x}(t),\ y(t) = \tilde{y}(t) + \hat{y}(t) \tag{17}$$

For an ac-dc converter, the steady-state component of each variable in general may include a dc, a fundamental, as well as a number of harmonics. According to the discussion in

Section II, a perturbation at frequency f_p in general may also produce small-signal responses at $f_p \pm nf_1$, with $n = 0, 1, 2, \ldots$. Based on this, each component included in (17) may be expressed by a complex Fourier series as follows, where the underline notation is used to denote the complex Fourier coefficients of each steady-state and small-signal variables:

$$\begin{aligned}
\tilde{x}(t) &= \Re e\left[\sum_{k=-\infty}^{\infty} \underline{X}_k e^{jk\omega_1 t}\right] \\
\hat{x}(t) &= \Re e\left[\sum_{k=-\infty}^{\infty} \underline{\widehat{X}}_k e^{j(\omega_p + k\omega_1)t}\right] \\
\tilde{y}(t) &= \Re e\left[\sum_{k=-\infty}^{\infty} \underline{Y}_k e^{jk\omega_1 t}\right] \\
\hat{y}(t) &= \Re e\left[\sum_{k=-\infty}^{\infty} \underline{\widehat{Y}}_k e^{j(\omega_p + k\omega_1)t}\right]
\end{aligned}$$

Note that the small-signal component is expressed using a single-sided Fourier series while the steady-state component uses a double-sided one. The reason for these different notations will become clear in the following development. Based on (17), the small-signal component of the bilinear function $z(t)$ can be calculated and expressed in the frequency domain as follows:

$$\begin{aligned}
\hat{z}(t) &= \tilde{y}(t)\hat{x}(t) + \tilde{x}(t)\hat{y}(t) \\
&= \Re e\left[\sum_{k=-\infty}^{\infty}\sum_{l=-\infty}^{\infty}\left\{\left(\underline{X}_k\underline{\hat{Y}}_l + \underline{Y}_l\underline{\hat{X}}_k\right)e^{j[\omega_p + (k+l)\omega_1]t}\right\}\right]
\end{aligned} \tag{18}$$

For each steady state and small signal component of $x(t)$ and $y(t)$, we define now a vector based on its complex Fourier coefficients:

$$\hat{x}(t): \begin{bmatrix} \vdots \\ \underline{\hat{X}}_{-2} \\ \underline{\hat{X}}_{-1} \\ \underline{\hat{X}}_0 \\ \underline{\hat{X}}_1 \\ \underline{\hat{X}}_2 \\ \vdots \end{bmatrix} \triangleq \hat{\mathbf{x}}, \quad \hat{y}(t): \begin{bmatrix} \vdots \\ \underline{\hat{Y}}_{-2} \\ \underline{\hat{Y}}_{-1} \\ \underline{\hat{Y}}_0 \\ \underline{\hat{Y}}_1 \\ \underline{\hat{Y}}_2 \\ \vdots \end{bmatrix} \triangleq \hat{\mathbf{y}} \tag{19}$$

$$\hat{x}(t): \begin{bmatrix} \vdots \\ \underline{\hat{X}}_{-2} \\ \underline{\hat{X}}_{-1} \\ \underline{\hat{X}}_0 \\ \underline{\hat{X}}_1 \\ \underline{\hat{X}}_2 \\ \vdots \end{bmatrix} \triangleq \hat{\mathbf{x}}, \quad \hat{y}(t): \begin{bmatrix} \vdots \\ \underline{\hat{Y}}_{-2} \\ \underline{\hat{Y}}_{-1} \\ \underline{\hat{Y}}_0 \\ \underline{\hat{Y}}_1 \\ \underline{\hat{Y}}_2 \\ \vdots \end{bmatrix} \triangleq \hat{\mathbf{y}} \tag{20}$$

The dimension of each vector defined in (19) and (20) is $2n+1$, n being the number of steady-state harmonics included in the analysis. The component occupying the center position of each vector is a dc component or at frequency f_p. Based on (18)-(20), the vector representing the Fourier coefficients of the small-signal component of the bilinear function $z = xy$ can be written as follows, where $\otimes$ indicates discrete convolution between two vectors:

$$\hat{\mathbf{z}} = \mathbf{y} \otimes \hat{\mathbf{x}} + \mathbf{x} \otimes \hat{\mathbf{y}} \tag{21}$$

The convolution in (21) is arranged such that the component occupying a certain position in the resulting vector will be at the same frequency as that of the component occupying the same position in each of the small-signal vectors that are being convoluted.

Convolution and the vector equation (21) provide a compact form to define the bilinear function in the frequency domain. However, an equation involving convolution is difficult to work with algebraically. To facilitate algebraic manipulation, we define a Toeplitz matrix [47] for each of the steady-state harmonic vectors $\mathbf{x}$ and $\mathbf{y}$ as follows:

$$\mathbf{X} = \begin{bmatrix} \ddots & \vdots & \iddots \\ \underline{X}_0 & \underline{X}_{-1} & \underline{X}_{-2} & \underline{X}_{-3} & \underline{X}_{-4} & \\ \underline{X}_1 & \underline{X}_0 & \underline{X}_{-1} & \underline{X}_{-2} & \underline{X}_{-3} & \\ \cdots \underline{X}_2 & \underline{X}_1 & \underline{X}_0 & \underline{X}_{-1} & \underline{X}_{-2} & \cdots \\ \underline{X}_3 & \underline{X}_2 & \underline{X}_1 & \underline{X}_0 & \underline{X}_{-1} & \\ \underline{X}_4 & \underline{X}_3 & \underline{X}_2 & \underline{X}_1 & \underline{X}_0 & \\ \iddots & \vdots & \ddots \end{bmatrix} \tag{22}$$

$$\mathbf{Y} = \begin{bmatrix} \ddots & \vdots & \iddots \\ \underline{Y}_0 & \underline{Y}_{-1} & \underline{Y}_{-2} & \underline{Y}_{-3} & \underline{Y}_{-4} & \\ \underline{Y}_1 & \underline{Y}_0 & \underline{Y}_{-1} & \underline{Y}_{-2} & \underline{Y}_{-3} & \\ \cdots \underline{Y}_2 & \underline{Y}_1 & \underline{Y}_0 & \underline{Y}_{-1} & \underline{Y}_{-2} & \cdots \\ \underline{Y}_3 & \underline{Y}_2 & \underline{Y}_1 & \underline{Y}_0 & \underline{Y}_{-1} & \\ \underline{Y}_4 & \underline{Y}_3 & \underline{Y}_2 & \underline{Y}_1 & \underline{Y}_0 & \\ \iddots & \vdots & \ddots \end{bmatrix} \tag{23}$$

This allows (21) to be rewritten as follows

$$\hat{\mathbf{z}} = \mathbf{Y}\hat{\mathbf{x}} + \mathbf{X}\hat{\mathbf{y}} \tag{24}$$

To convert the phase-a current model (15) into the frequency domain using this method, denote the steady-state variables involved in the model as follows:

$$\tilde{v}_a = V_1 \cos(\omega_1 t + \varphi_{v1}) \tag{25}$$

$$\tilde{i}_a = I_1 \cos(\omega_1 t + \varphi_{i1}) \tag{26}$$

$$\tilde{d}_a = D_1 \cos(\omega_1 t + \varphi_{d1}) \tag{27}$$

Note that $\{V_1,\ I_1,\ D_1\}$ are the magnitude of the phase voltage, current and duty ratio, respectively. For convenience, each of these steady-state variables can be expressed as a

complex number (phasor) defined as follows:

$$\underline{V}_1 = V_1 e^{j\varphi_{v1}},\ \underline{I}_1 = I_1 e^{j\varphi_{i1}},\ \underline{D}_1 = D_1 e^{j\varphi_{d1}} \tag{28}$$

Similar to (20), a small-signal vector can be defined for each of the small-signal variables $\{\hat{i}_a,\ \hat{d}_a,\ \hat{v}_{dc},\ \hat{v}_a\}$ involved in (15). These vectors will be denoted as $\{\hat{\mathbf{i}}_a,\ \hat{\mathbf{d}}_a,\ \hat{\mathbf{v}}_{dc},\ \hat{\mathbf{v}}_a\}$. Based on (25)-(27), a Toeplitz matrix can be formulated for each of the steady-state variables $\tilde{v}_a$, $\tilde{i}_a$ and $\tilde{d}_a$. Denote them as $\mathbf{V}_a$, $\mathbf{I}_a$ and $\mathbf{D}_a$, respectively. Based on these definitions, the right-hand side of (16) can be expressed in the frequency domain as

$$\mathbf{D}_a\hat{\mathbf{v}}_{dc} + V_{dc}\hat{\mathbf{d}}_a - \hat{\mathbf{v}}_a - \hat{\mathbf{v}}_{cm}. \tag{29}$$

Similarly, the left-hand of (16) becomes $\mathbf{Z}_l\hat{\mathbf{i}}_a$ in the frequency domain, $\mathbf{Z}_l$ being a diagonal impedance matrix:

$$\mathbf{Z}_l = j2\pi L \cdot diag\left[\{\cdots, f_p - f_1, f_p, f_p + f_1, \cdots\}\right] \tag{30}$$

Based on the harmonic balance principle [48], the coefficients of components at the same frequency on the two sides of the resulting algebraic equation should be equal. This leads to the following algebraic equation:

$$\mathbf{Z}_l\hat{\mathbf{i}}_a = \mathbf{D}_a\hat{\mathbf{v}}_{dc} + V_{dc}\hat{\mathbf{d}}_a - \hat{\mathbf{v}}_a - \hat{\mathbf{v}}_{cm} \tag{31}$$

Each of the differential equations in the converter circuit and control model can be converted to the frequency domain by this method. The resulting algebraic models together form a complete frequency-domain model of the converter. The model can then be used to determine different components of the converter current response to a voltage perturbation at ac or dc port. The required immittance models can then be determined based on the corresponding current responses.

The general formulation introduced in (17)-(24) assumed an arbitrary number of frequency components. In a two-level VSC, steady state operation can be assumed free of harmonics on the ac side and ripple-free on the dc side, as indicated by (25)-(27). This also limits the small-signal components to frequencies $\{f_p - 2f_1, f_p - f_1, f_p, f_p + f_1, f_p + 2f_1\}$ only, as explained early in this section. Based on this, the dimension of each frequency-domain model can be limited to five by considering only the five small-signal response frequencies listed above and the dc, the fundamental and the second harmonic in the steady-state response. (The second steady-state harmonics actually do not exist, but are included to match the dimension of the small-signal vectors.)

The method has been explained so far by assuming a bilinear function, but is applicable to any nonlinear function. For example, consider a general nonlinear function $g(x, y)$. Denote the partial derivative of this function relative to x and y as $g_x(x,\ y)$ and $g_y(x, y)$, respectively. Using the steady-state and small-signal notations introduced before, we can write the small-signal response of $g(x, y)$ in the time and frequency domain as follows where $\mathbf{g}_x$ and $\mathbf{g}_y$ are defined by the steady-state spectra of the partial derivative functions $\tilde{g}_x$ and $\tilde{g}_y$, and $\mathbf{G}_x$ and $\mathbf{G}_y$ are Toeplitz matrices corresponding to $\mathbf{g}_x$ and $\mathbf{g}_y$, respectively:

$$\hat{g}(t) = \tilde{g}_x\left[\tilde{x}(t),\ \tilde{y}(t)\right]\hat{x}(t) + \tilde{g}_y\left[\tilde{x}(t),\ \tilde{y}(t)\right]\hat{y}(t) \tag{32}$$

$$\hat{\mathbf{g}} = \mathbf{g}_x \otimes \hat{\mathbf{x}} + \mathbf{g}_y \otimes \hat{\mathbf{y}} = \mathbf{G}_x\hat{\mathbf{x}} + \mathbf{G}_y\hat{\mathbf{y}} \tag{33}$$

IV. IMMITTANCE MODEL DEVELOPMENT

This section presents analytical models for the immittances defined in Table I. The first two subsections model the converter power stage and control in response to an ac-port voltage perturbation. The models are combined in Section IV.C to give analytical models for $\{Y_{pp},\ Y_{pd},\ Y_{pn}\}$. A general relationship between positive- and negative-sequence variables and immittances is then established and used to define $\{Y_{nn},\ Y_{nd},\ Y_{np}\}$ based on $\{Y_{pp},\ Y_{pd},\ Y_{pn}\}$. The power stage and control models are then modified to develop Y_{dd} , Y_{dp} and Y_{dn} in the last subsection.

A. POWER STAGE RESPONSE TO AC-PORT PERTURBATION

To start, assume the voltage perturbation applied at the ac port (phase a) is $\hat{v}_a(f_p) = \hat{V}_p\cos(\omega_p t + \varphi_p)$. The magnitude $\hat{V}_p$ is small compared to the fundamental. The initial phase angle φ_p does not affect the final model and can be set to zero. Using the notations introduced in the last section, $\hat{v}_a(f_p)$ can be expressed in the frequency domain as

$$\hat{\mathbf{v}}_a = \begin{bmatrix} 0 \\ 0 \\ \underline{\hat{V}}_a \\ 0 \\ 0 \end{bmatrix} = \begin{bmatrix} 0 \\ 0 \\ \hat{V}_p e^{j\varphi_p} \\ 0 \\ 0 \end{bmatrix}. \tag{34}$$

The sequence of the voltage perturbation is not reflected in this vector but it affects the converter circuit and control models, as will be seen later. Recall that small-signal variables are represented by single-sided Fourier series.

The dc bus voltage is treated as constant when modeling the two-port network with a voltage perturbation at the ac port, which means $\hat{\mathbf{v}}_{dc} = 0$. This assumption also renders the power stage model (1) linear and (2) unnecessary. However, to be consistent with the control model, which is nonlinear and requires linearization, we will still use small-signal variables in the power stage model. Since the ac port corresponds to phase a, we only need a frequency-domain model for phase-a current, which can be obtained from the general model (31) by removing the $\hat{\mathbf{v}}_{dc}$ term and reducing the dimension of each vector to five based on the actual number of small-signal components considered. The resulting model is

$$\mathbf{Z}_l\hat{\mathbf{i}}_a = V_{dc}\hat{\mathbf{d}}_a - \hat{\mathbf{v}}_a - \hat{\mathbf{v}}_{cm}. \tag{35}$$

Accordingly, $\mathbf{Z}_l$ is also reduced to a 5×5 matrix and is redefined as follows:

$$\mathbf{Z}_l = j2\pi L \cdot diag\left[\{f_{p-2}, f_{p-1}, f_p, f_{p+1}, f_{p+2}\}\right] \tag{36}$$

All variables in (35) are related to phase a except for the common-mode voltage v_{cm}, which depends on other phases:

$$v_{cm} = \frac{d_a + d_b + d_c}{3} \cdot v_{dc} \tag{37}$$

Therefore, (35) cannot be used alone to model the converter power stage unless v_{cm} is removed or made independent of other two phases, namely, d_b and d_c. Simply dropping this term from (35) is not permitted because it will cause the model to predict small-signal current responses in the zero sequence that in actuality cannot flow. To make v_{cm} mathematically independent of other two phases, we can express d_b and d_c in terms of d_a based on the sequence relationship among their steady-state and small-signal components. This is possible but increases the complexity of the model.

The approach taken here is to remove $\hat{\mathbf{v}}_{cm}$ from (35) and at the same time modify the remaining of the equation such that any zero-sequence component of $\hat{\mathbf{i}}_a$ is forced to be zero. As can be seen from (35) and (36), a component of $\hat{\mathbf{i}}_a$ may be forced to be zero by making the corresponding diagonal element of $\mathbf{Z}_l$ infinite. For example, the current at frequency $f_p - f_1$ will remain zero regardless the voltage on the right-hand side if $\mathbf{Z}_l$ is changed to

$$j2\pi L \cdot \text{diag}\left[\{f_p - 2f_1, \infty, f_p, f_p + f_1, f_p + 2f_1\}\right].$$

Because infinite is difficult to work with in equations, we rewrite (35) as follows to use admittance of the inductor:

$$\hat{\mathbf{i}}_a = \mathbf{Y}_l\left(V_{dc}\hat{\mathbf{d}}_a - \hat{\mathbf{v}}_a - \hat{\mathbf{v}}_{cm}\right) \tag{38}$$

$$\mathbf{Y}_l = \frac{1}{j2\pi L} diag\left[\left\{\frac{1}{f_{p-2}}, \frac{1}{f_{p-1}}, \frac{1}{f_p}, \frac{1}{f_{p+1}}, \frac{1}{f_{p+2}}\right\}\right] \tag{39}$$

In this form, a component of $\hat{\mathbf{i}}_a$ is forced to be zero if the corresponding diagonal element of $\mathbf{Y}_l$ is set to zero.

To determine which of the five frequency components of $\hat{\mathbf{i}}_a$ may be in the zero sequence (common mode), first recall from Section II that ac-port current responses at the perturbation frequency are always in the same sequence as the voltage perturbation. Therefore, the component at f_p is not in the zero sequence. Recall also that a small-signal response at $f_p \pm f_1$ or $f_p \pm 2f_1$ is generated when a variable at f_p is multiplied (twice for $f_p \pm 2f_1$) with another variable at the fundamental frequency. Denote the phase angle of the small signal and the fundamental of phase a variables as φ_p and φ_1, respectively. Based on trigonometric relations, the response at $f_p + nf_1$ carries phase angle $\varphi_a = \varphi_p + n\varphi_1$, $n = \pm 1, \pm 2$. Since both the fundamental and the perturbation are balanced among the three phases, the initial phase of the variable in phase b and c at the same frequency can be written as follows:

- With a positive-sequence perturbation:

$$\varphi_b = \left(\varphi_p - \frac{2\pi}{3}\right) + n\left(\varphi_1 - \frac{2\pi}{3}\right)$$
$$\varphi_c = \left(\varphi_p + \frac{2\pi}{3}\right) + n\left(\varphi_1 + \frac{2\pi}{3}\right)$$

TABLE II: Sequences of Small-Signal Responses to an AC-Port Voltage Perturbation

	f_{p-2}	f_{p-1}	f_p	f_{p+1}	f_{p+2}
PS Perturbation	NS	ZS	PS	NS	ZS
NS Perturbation	ZS	PS	NS	ZS	PS

- With a negative-sequence perturbation:

$$\varphi_b = \left(\varphi_p + \frac{2\pi}{3}\right) + n\left(\varphi_1 - \frac{2\pi}{3}\right)$$
$$\varphi_c = \left(\varphi_p - \frac{2\pi}{3}\right) + n\left(\varphi_1 + \frac{2\pi}{3}\right)$$

From these phase relations, the sequence of the response at $f_p + nf_1$ can be determined as summarized in Table II where the first column indicates the sequence of the applied voltage perturbation, and PS, NS and ZS stands for positive, negative, and zero sequence, respectively.

Based on Table II and the method discussed before, we can now rewrite the frequency-domain model (38) as follows to remove the common-mode voltage $\hat{\mathbf{v}}_{cm}$:

$$\hat{\mathbf{i}}_a = \mathbf{Y}_l\left(V_{dc}\hat{\mathbf{d}}_a - \hat{\mathbf{v}}_a\right) \tag{40}$$

The admittance matrix $\mathbf{Y}_l$ in (40) is to be replaced by

$$\mathbf{Y}_{lp} = \frac{1}{j2\pi L} diag\left[\left\{\frac{1}{f_{p-2}}, 0, \frac{1}{f_p}, \frac{1}{f_{p+1}}, 0\right\}\right] \tag{41}$$

if the applied ac-port voltage perturbation is in the positive sequence, and by

$$\mathbf{Y}_{ln} = \frac{1}{j2\pi L} diag\left[\left\{0, \frac{1}{f_{p-1}}, \frac{1}{f_p}, 0, \frac{1}{f_{p+2}}\right\}\right] \tag{42}$$

if the voltage perturbation is in the negative sequence.

To complete the power stage model, we also need to define the Toeplitz matrix for each of the state and control variables. Since v_{dc} is held constant when ac-port voltage perturbation is applied, we only need to do this for the phase-a current i_a and duty ratio d_a. According to the harmonic-free assumption stated before, the phase-a duty ratio (d_a) and current (i_a) each contains only the fundamental component (in the positive sequence). Each of these fundamental components has been specified in (28) by a complex number. Following the general definition introduced before, the Toeplitz matrices corresponding to $\{d_a, i_a\}$ can be written as follows, where the asterisk superscript $*$ indicates complex conjugation:

$$\mathbf{D}_a = \frac{1}{2}\begin{bmatrix} 0 & \underline{D}_1^* & 0 & 0 & 0 \\ \underline{D}_1 & 0 & \underline{D}_1^* & 0 & 0 \\ 0 & \underline{D}_1 & 0 & \underline{D}_1^* & 0 \\ 0 & 0 & \underline{D}_1 & 0 & \underline{D}_1^* \\ 0 & 0 & 0 & \underline{D}_1 & 0 \end{bmatrix} \tag{43}$$

$$\mathbf{I}_a = \frac{1}{2}\begin{bmatrix} 0 & \underline{I}_1^* & 0 & 0 & 0 \\ \underline{I}_1 & 0 & \underline{I}_1^* & 0 & 0 \\ 0 & \underline{I}_1 & 0 & \underline{I}_1^* & 0 \\ 0 & 0 & \underline{I}_1 & 0 & \underline{I}_1^* \\ 0 & 0 & 0 & \underline{I}_1 & 0 \end{bmatrix} \tag{44}$$

Recall that steady-state variables are expressed by double-sided Fourier series, which leads to the 1/2 factor in front of each matrix.

The last equation needed to complete the power stage model is the small-signal response of i_{dc}, the current flowing into the dc port of the converter, as defined in Fig. 1. Based on the operation principle of the converter, this current is related to the ac phase currents and duty ratios by

$$i_{dc} = d_a i_a + d_b i_b + d_c i_c.$$

Using the same procedure, the corresponding frequency-domain model is given in (45) where $\{\mathbf{D}_b,\ \mathbf{D}_c,\ \mathbf{I}_b,\ \mathbf{I}_c\}$ and $\{\hat{\mathbf{d}}_b,\ \hat{\mathbf{d}}_c,\ \hat{\mathbf{i}}_b,\ \hat{\mathbf{i}}_c\}$ are the Toeplitz matrices and small-signal vectors of phase-b and phase-c duty ratios and currents:

$$\hat{\mathbf{i}}_{dc} = \left(\mathbf{D}_a\hat{\mathbf{i}}_a + \mathbf{I}_a\hat{\mathbf{d}}_a\right) + \left(\mathbf{D}_b\hat{\mathbf{i}}_b + \mathbf{I}_b\hat{\mathbf{d}}_b\right) + \left(\mathbf{D}_c\hat{\mathbf{i}}_c + \mathbf{I}_c\hat{\mathbf{d}}_c\right) \tag{45}$$

Based on the sequence relationship identified before for steady state and small-signal components among the three phases and at different frequencies, $\{\mathbf{D}_b,\ \mathbf{D}_c,\ \mathbf{I}_b,\ \mathbf{I}_c\}$ and $\{\hat{\mathbf{d}}_b,\ \hat{\mathbf{d}}_c,\ \hat{\mathbf{i}}_b,\ \hat{\mathbf{i}}_c\}$ can be eliminated from (45) by expressing each in terms of $\{\mathbf{D}_a,\ \mathbf{I}_a\}$ and $\{\hat{\mathbf{d}}_a,\ \hat{\mathbf{i}}_a\}$. The result is a model of $\hat{\mathbf{i}}_{\mathrm{dc}}$ that depends only on phase-a variables, as given below:

$$\hat{\mathbf{i}}_{dc} = \frac{3}{2}\begin{bmatrix} 0 & 0\,0 & 0 & 0 \\ \underline{D}_1 & 0\ \underline{D}_1^* & 0 & 0 \\ 0 & 0\,0 & 0 & 0 \\ 0 & 0\,0 & 0 & 0 \\ 0 & 0\,0 & \underline{D}_1 & 0 \end{bmatrix}\hat{\mathbf{i}}_a + \frac{3}{2}\begin{bmatrix} 0 & 0\,0 & 0 & 0 \\ \underline{I}_1 & 0\ \underline{I}_1^* & 0 & 0 \\ 0 & 0\,0 & 0 & 0 \\ 0 & 0\,0 & 0 & 0 \\ 0 & 0\,0 & \underline{I}_1 & 0 \end{bmatrix}\hat{\mathbf{d}}_a \tag{46}$$

B. CONTROL RESPONSE TO AC-PORT PERTURBATION

The purpose of control modeling is to relate the duty ratio $\hat{\mathbf{d}}_a$ to other variables involved in the power stage model. In general, the linearized control model can be expressed as

$$\hat{\mathbf{d}}_a = \mathbf{Q}\hat{\mathbf{i}}_a + \mathbf{P}\hat{\mathbf{v}}_a + \mathbf{E}\hat{\mathbf{v}}_{dc}. \tag{47}$$

Matrix $\mathbf{Q}$ models the dependency of the duty ratio on the ac-port current and is determined by current control of the converter. The duty ratio is also affected by the ac-port voltage when a PLL (or ac voltage control) is used, and the effects are captured by matrix $\mathbf{P}$. Matrix $\mathbf{E}$ models the effects of dc bus voltage control. Because the dc bus voltage is held constant when ac-port voltage is perturbed, this term can be ignored, such that the control model assumes a simpler form:

$$\hat{\mathbf{d}}_a = \mathbf{Q}\hat{\mathbf{i}}_a + \mathbf{P}\hat{\mathbf{v}}_a \tag{48}$$

The control architecture assumed in Fig. 1 is similar to that of the MMC modeled in [38]. Therefore, the control models developed in [38] for MMC can be adopted for use here. For easy reference, we will give the resulting matrix $\mathbf{Q}$ and $\mathbf{P}$ here with a brief explanation. Readers are referred to [38] for more detailed development of each matrix.

The dq-frame current control defined in Fig. 1(b) use a PI regulator in each axis and includes a decoupling term between the two axes. The decoupling gain is denoted as K_d and the PI regulator transfer function is defined as $H_i(s)$. Since this is a linear control, the response of the control output (duty ratio) at a given frequency depends on ac-port current at the same frequency. Therefore, $\mathbf{Q}$ is a diagonal matrix and is defined as follows, where K_m is the gain of the modulator, that is, the gain from the control output m_a to duty ratio d_a:

$$\mathbf{Q} = K_m \cdot diag\left[\{q_k\}|_{k\in[-2,\ 2]}\right] \tag{49}$$

The dq transformation creates a frequency rotation that depends on the sequence of the currents. This causes the matrix to be different between positive- and negative-sequence perturbations. For a positive-sequence perturbation, the diagonal elements are defined as follows:

$$q_k = |\mathrm{mod}\,(k+1,\ 3)| \cdot \{\mathrm{mod}\,(k+1,\ 3)\,jK_d - H_i\left[j2\pi\left(f_p + kf_1\right) - mod\,(k+1,\ 3)\,j2\pi f_1\right]\} \tag{50}$$

Function $\mathrm{mod}(k,\ 3)$ is a modified modulo-3 function defined as follows where m is an integer:

$$\mathrm{mod}\,(k,\ 3) = \begin{cases} +1 & k = 3m+1 \\ -1 & k = 3m-1 \\ 0 & k = 3m \end{cases}$$

For a negative-sequence impedance, the diagonal elements of $\mathbf{Q}$ are slightly different, as given below:

$$q_k = |\mathrm{mod}\,(k-1,\ 3)| \cdot \{\mathrm{mod}\,(k-1,\ 3)\,jK_d - H_i\left[j2\pi\left(f_p + kf_1\right) - mod\,(k-1,\ 3)\,j2\pi f_1\right]\} \tag{51}$$

The dq transformation used by the PLL in Fig. 1(d) creates a similar frequency rotation, as can be concluded from (10). Namely, with a voltage perturbation at frequency f_p, the frequency of angle perturbation at the PLL output is $f_p - f_1$ if the perturbation is in the positive sequence, and $f_p + f_1$ if it is in the negative sequence. The angle perturbation contributes to the response of the duty ratio at the perturbation frequency as well as at $f_p - 2f_1$ or $f_p + 2f_1$, depending on the sequence of the voltage perturbation. The duty ratio response at $f_p \pm 2f_1$ is an additional source for the second current response discussed in Section II and causes matrix $\mathbf{P}$ to have a non-zero off-diagonal element [38]. In a general form, $\mathbf{P}$ can be written as

$$\mathbf{P} = \left[p_{(i,j)_i,\ j\in[-2,\ 2]}\right]. \tag{52}$$

All elements of $\mathbf{P}$ are zero except for two, which are defined in the following:

- With a positive-sequence voltage perturbation:

$$p_{(0,\,0)} = \frac{\underline{D}_1 + K_m \underline{I}_1 \left[H_i\left(j\omega_{p-1}\right) - jK_{id}\right]}{2} \cdot \frac{G_\theta\left[j\omega_{p-1}\right]}{\underline{V}_1} \tag{53}$$

$$p_{(-2,\,0)} = -\frac{\underline{D}_1^* + K_m \underline{I}_1^* \left[H_i\left(j\omega_{p-1}\right) + jK_{id}\right]}{2} \cdot \frac{G_\theta\left[j\omega_{p-1}\right]}{\underline{V}_1} \tag{54}$$

- With a negative-sequence voltage perturbation:

$$p_{(0,\,0)} = \frac{\underline{D}_1^* + K_m \underline{I}_1^* \left[H_i\left(j\omega_{p+1}\right) + jK_{id}\right]}{2} \cdot \frac{G_\theta\left[j\omega_{p+1}\right]}{\underline{V}_1^*} \tag{55}$$

$$p_{(2,\,0)} = -\frac{\underline{D}_1 + K_m \underline{I}_1 \left[H_i\left(j\omega_{p+1}\right) - jK_{id}\right]}{2} \cdot \frac{G_\theta\left[j\omega_{p+1}\right]}{\underline{V}_1^*} \tag{56}$$

Function G_θ used in (53)-(56) is the PLL closed-loop gain and is defined as follows, where $H_\theta(s)$ is the transfer function of the PI compensator, as shown in Fig. 1(d), and $T_\theta(s)$ defines the loop gain of the PLL:

$$G_\theta(s) = \frac{T_\theta(s)}{1+T_\theta(s)},\; T_\theta(s) = \sqrt{\frac{3}{2}} V_1 \frac{H_\theta(s)}{s} \tag{57}$$

Recall from (28) that $\underline{V}_1$, $\underline{I}_1$ and $\underline{D}_1$ are phasors at the fundamental frequency that define the steady-state operation "point" of the converter. Since $\underline{D}_1 V_{dc}$ is the fundamental of the converter PWM output voltage (measured at the point between the upper and lower switch of each phase leg), the three phasors are also related to each other as follows where $\underline{V}_{1L}$ is the fundamental voltage across the filter inductor:

$$\underline{D}_1 V_{dc} = j\omega_1 L \underline{I}_1 + \underline{V}_1 \triangleq \underline{V}_{1L} + \underline{V}_1$$

C. ANALYTICAL MODELS OF $\{Y_{pp}, Y_{pd}, Y_{pn}\}$

Equations (40) and (48) form a complete frequency-domain model of the converter for the case when a voltage perturbation is applied to the ac port. Substituting $\hat{\mathbf{d}}_a$ in (40) by (48), we have

$$\hat{\mathbf{i}}_a = V_{dc}\mathbf{Y}_l\hat{\mathbf{d}}_a - \mathbf{Y}_l\hat{\mathbf{v}}_a = V_{dc}\mathbf{Y}_l\left(\mathbf{Q}\hat{\mathbf{i}}_a + \mathbf{P}\hat{\mathbf{v}}_\mathbf{a}\right) - \mathbf{Y}_l\hat{\mathbf{v}}_a.$$

This gives the following solution for $\hat{\mathbf{i}}_a$, where $\mathbf{U}$ is a 5×5 unity matrix:

$$\hat{\mathbf{i}}_a = \left(\mathbf{U} - V_{dc}\mathbf{Y}_l\mathbf{Q}\right)^{-1}\mathbf{Y}_l\left(V_{dc}\mathbf{P} - \mathbf{U}\right)\hat{\mathbf{v}}_a$$

This solution can be put back in (48) to determine $\hat{\mathbf{d}}_a$. The dc-port current response $\hat{\mathbf{i}}_{\rm dc}$ can then be determined from (46). The first six self admittances and transfer admittances defined in Table I can then be determined as transfer functions from the corresponding component of $\hat{\mathbf{i}}_a$ and $\hat{\mathbf{i}}_{dc}$ to the applied ac-port voltage perturbation.

Since matrices $\mathbf{Y}_l$, $\mathbf{P}$ and $\mathbf{Q}$ are sequence-dependent, we need to form and solve a separate set of algebraic equations to find $\hat{\mathbf{i}}_a$ and $\hat{\mathbf{i}}_{\rm dc}$ for each case. Recall from Section IV.B that $\hat{\mathbf{i}}_a$ is composed of small-signal responses of phase-a current at different frequencies:

$$\hat{\mathbf{i}}_a = \begin{bmatrix} \hat{\underline{I}}_{a-2} & f_p - 2f_1 \\ \hat{\underline{I}}_{a-1} & f_p - f_1 \\ \hat{\underline{I}}_{a} & f_p \\ \hat{\underline{I}}_{a+1} & f_p + f_1 \\ \hat{\underline{I}}_{a+2} & f_p + 2f_1 \end{bmatrix} \tag{58}$$

With a positive-sequence perturbation, the solved $\hat{\mathbf{i}}_a$ vector has two non-zero elements, occupying the first and third position from the top. This indicates that a positive-sequence perturbation to the ac-port voltage only produces current response at f_p and $f_p - 2f_1$, as concluded from the qualitative analysis presented in Section II. The sequence of each of these two current responses is indicated in Table II and is also consistent with the conclusion developed in Section II. The ratio of $\widehat{\underline{I}_a}$ and $\widehat{\underline{I}_{a-2}}$ defined in (58) to the voltage perturbation $\widehat{\underline{V}_a}$ (34) gives the self admittance Y_{pp} and transfer admittance Y_{pn}, respectively. For the dc-port current, it can be seen from (46) that only the component at $f_p - f_1$ is non-zero because $\hat{\mathbf{i}}_a$ and $\hat{\mathbf{d}}_a$ have no response at frequency $f_p + 2f_1$. This non-zero current defines the transfer admittance Y_{pd}.

With some algebraic manipulation, the analytical models (59)-(61) given below are obtained for admittances Y_{pp}, Y_{pd} and Y_{pn} where $s = j2\pi f_p$.

$$Y_{pp}(s) = \frac{1 - \frac{G_\theta(s_{-1})}{2\underline{V}_1}\left\{\underline{I}_1\left[H_{i0}(s_{-1}) - jK_{d0}\right] + \underline{D}_1 V_{dc}\right\}}{sL + \left[H_{i0}(s - j\omega_1) - jK_{d0}\right]} \tag{59}$$

$$Y_{pn}(s) = \frac{\frac{G_\theta(s_{-1})}{2\underline{V}_1}\left\{\underline{I}_1^*\left[H_{i0}(s - j\omega_1) + jK_{d0}\right] + \underline{D}_1^* V_{dc}\right\}}{(s - j2\omega_1)L + \left[H_{i0}(s - j\omega_1) + jK_{d0}\right]} \tag{60}$$

$$Y_{pd}(s) = \frac{3}{2V_{dc}}\frac{\underline{V}_1^* - \underline{I}_1^* H_{i0}(s - j\omega_1)}{H_{i0}(s - j\omega_1) + (s - j\omega_1)L} + \frac{jQG_\theta(s - j\omega_1)}{\underline{V}_1 V_{dc}}\frac{H_{i0}(s - j\omega_1) - (s - j\omega_1)L}{H_{i0}(s - j\omega_1) + (s - j\omega_1)L} \tag{61}$$

Most symbols used in (59)-(61) have been defined and used before except Q, which is the reactive power output of the converter. To shorten the expressions, the following variables are defined for the current compensator and are used:

$$H_{i0}(s) = K_m V_{dc} H_i(s),\; K_{d0} = K_m V_{dc} K_d \tag{62}$$

Additionally, $K_{d0} = \omega_1 L$ is assumed in (61). The model is more complex without this assumption. However, the other two models do not involve this assumption.

D. MODELING OF $\{Y_{nn},\ Y_{nd},\ Y_{np}\}$

The procedure outlined above can be repeated for a negative-sequence perturbation to find Y_{nn}, Y_{nd} and Y_{np}. As an alternative approach, we will develop these transfer functions from Y_{pp}, Y_{pd} and Y_{pn} by taking advantage of a relationship between positive and negative sequence. This also helps to reduce the number of independent models from nine to six.

The relationship is based on the observation that a cosine function remains unchanged if both its frequency and initial phase angle change sign at the same time:

$$x\cos(\omega t+\varphi)=x\cos((-\omega)t-\varphi) \tag{63}$$

For mathematical convenience, define $\underline{X}=xe^{j\varphi}$ and express the cosine function in a more abstract form as $\omega,\ \underline{X}$. Based on this notation, the relationship (63) can be expressed as

$$\langle\omega,\ \underline{X}\rangle=\langle-\omega,\ \underline{X}^*\rangle. \tag{64}$$

For three-phase signals, (64) applies to each phase. The phase angle reversal also causes the sequence to change, such that a balanced three-phase in the positive sequence at frequency ω becomes negative sequence at frequency $-\omega$, and vice versa, as can be seen from the following equation:

$$\begin{bmatrix} x\cos(\omega t+\varphi) \\ x\cos\left(\omega t+\varphi-\frac{4\pi}{3}\right) \\ x\cos\left(\omega t+\varphi-\frac{2\pi}{3}\right)\end{bmatrix}=\begin{bmatrix} x\cos((-\omega)t-\varphi) \\ x\cos\left((-\omega)t-\varphi+\frac{4\pi}{3}\right) \\ x\cos\left((-\omega)t-\varphi+\frac{2\pi}{3}\right)\end{bmatrix}$$

To express this relationship in a mathematical form, we expand the definition $\omega,\ \underline{X}$ by adding a third argument σ to indicate the sequence. Additionally, we use $\bar{\sigma}$ to denote a sequence that is opposite to σ (e.g., if $\sigma=$ positive sequence, then $\bar{\sigma}=$ negative sequence). The relationship among three-phase signals can then be expressed mathematically as

$$\langle\omega,\ \underline{X},\ \sigma\rangle=\langle-\omega,\ \underline{X}^*,\ \bar{\sigma}\rangle. \tag{65}$$

Based on the notations introduced before, a negative-sequence perturbation to the ac port voltage can be written as $\omega_p,\ \hat{V}_p e^{j\varphi_p},\ \mathrm{NS}$, where NS indicate negative sequence. According to (65), this can also be treated as a positive-sequence perturbation at $-\omega_p$ and be written as follows:

$$\langle-\omega_p,\ \hat{V}_p e^{-j\varphi_p},\ \mathrm{PS}\rangle \tag{66}$$

As a positive-sequence perturbation, (66) will generate two current responses: one at $-\omega_p$ in the positive sequence, and one at $-\omega_p-2\omega_1$ in the negative sequence. Each of these currents can be determined by multiplying the voltage perturbation (66) with the corresponding admittance:

$$\hat{\underline{I}}_a\left(-\omega_p\right)=-Y_{pp}\left(-j\omega_p\right)\hat{V}_p e^{-j\varphi_p}$$
$$\hat{\underline{I}}_{a-2}\left(-\omega_p-2\omega_1\right)=-Y_{pn}\left(-j\omega_p\right)\hat{V}_p e^{-j\varphi_p}$$

Applying (65) to each of these currents, we have

$$\begin{aligned}&\langle-\omega_p,\ -Y_{pp}\left(-j\omega_p\right)\hat{V}_p e^{-j\varphi_p},\ \mathrm{PS}\rangle \\ &=\langle\omega_p,\ -Y_{pp}^*\left(-j\omega_p\right)\hat{V}_p e^{j\varphi_p},\ \mathrm{NS}\rangle\end{aligned} \tag{67}$$

$$\begin{aligned}&\langle-\omega_p-2\omega_1,\ -Y_{pn}\left(-j\omega_p\right)\hat{V}_p e^{-j\varphi_p},\ \mathrm{NS}\rangle \\ &=\langle\omega_p+2\omega_1,\ -Y_{pn}^*\left(-j\omega_p\right)\hat{V}_p e^{j\varphi_p},\ \mathrm{PS}\rangle\end{aligned} \tag{68}$$

The right-hand side of (67) in effect defines a negative-sequence current at frequency ω_p, which is the expected current response to the original negative-sequence voltage perturbation. The ratio of this current to the original negative-sequence voltage perturbation $\hat{V}_p e^{j\varphi_p}$ is what we have defined as admittance Y_{nn}. Therefore, this current can also be written as $\omega_p,\ -Y_{nn}(j\omega_p)\hat{V}_p e^{j\varphi_p},\ \mathrm{NS}$. By comparing this with the right-hand side of (67), we conclude that

$$Y_{nn}(s)=Y_{pp}^*(-s). \tag{69}$$

Similarly, the right-hand side of (68) corresponds to a positive-sequence response at frequency $\omega_p+2\omega_1$, which is the expected second current response to a negative-sequence voltage perturbation. The ratio of this current to the original negative-sequence voltage perturbation $\hat{V}_p e^{j\varphi_p}$ is what we have defined as transfer admittance Y_{np}. Therefore, this current can also be written as

$$\langle\,\omega_p+2\omega_1,\ -Y_{np}\left(j\omega_p\right)\hat{V}_p e^{j\varphi_p},\ \mathrm{PS}\rangle.$$

By comparing this with the right-hand side of (68), we conclude that

$$Y_{np}(s)=Y_{pn}^*(-s). \tag{70}$$

By similar analyses, we can also conclude that

$$Y_{nd}(s)=Y_{pd}^*(-s). \tag{71}$$

Equations (69)-(71) are general and allow the self and transfer admittances associated with a negative-sequence perturbation to be obtained from the models developed for a positive-sequence perturbation. They reduce the total number of independent immittance models required for characterizing a three-phase ac-dc converter from nine to six.

E. MODELING OF Y_{dd}, Y_{dp}, AND Y_{dn}

Modeling of the converter's response to a dc-port voltage perturbation follows the same steps used in the last subsection. However, there are several noticeable differences that affect some parts of the model:

- The sequence of ac-port current responses is different from that identified in Table II, requiring the admittance matrix $\mathbf{Y}_l$ to be defined differently.
- The power stage model becomes nonlinear when the dc bus voltage is variable, hence has to be linearized first.
- With the ac-port voltage unperturbed, the PLL output is constant and can be ignored in the control model. On the other hand, dc bus voltage control has to be included.

Given the similar overall procedure, we will present the power stage and control models briefly for this case. To start, recall that a response at $f_p\pm f_1$ or $f_p\pm 2f_1$ is generated when a small-signal response at f_p or $f_p\pm f_1$ is multiplied with a fundamental component. Such a multiplication also shifts the

TABLE III: Sequences of Small-Signal Responses to a DC-Port Voltage Perturbation

f_p-2f_1	f_p-f_1	f_p	f_p+f_1	f_p+2f_1
PS	NS	ZS	PS	NS

phase angle, thereby changing the sequence among the three phases. However, with a perturbation at the dc port, the phase shift among the resulting three-phase responses does not have the additional phase shift of the perturbation as in the case of an ac-port perturbation. Therefore, the phase shift from phase a to b and from b to c among small-signal current responses at frequency f_p+nf_1 is simply $n\times(2\pi/3)$. Based on this, the sequence of the five small-signal currents included in $\hat{\mathbf{i}}_a$ can be determined as given in Table III.

Similar to (34), a dc-port voltage perturbation $\hat{v}_{dc}(f_p)=\hat{V}_p\cos(\omega_p t+\varphi_p)$ can be written as a vector:

$$\hat{\mathbf{v}}_{dc}=\begin{bmatrix}0\\0\\\hat{V}_p e^{j\varphi_p}\\0\\0\end{bmatrix}. \tag{72}$$

Based on this and the fact that $\hat{\mathbf{v}}_a=0$, the linearized phase-a current model in the frequency domain is

$$\hat{\mathbf{i}}_a=\mathbf{Y}_{ld}\left(V_{dc}\hat{\mathbf{d}}_a+\mathbf{D}_a\hat{\mathbf{v}}_{dc}\right) \tag{73}$$

where $\mathbf{D}_a$ has been defined before in (43) and the admittance matrix $\mathbf{Y}_{ld}$ is modified from (39) according to Table III to force the zero-sequence current at frequency f_p to zero when the common-mode voltage v_{cm} is removed:

$$\mathbf{Y}_{ld}=\frac{1}{j2\pi L}diag\left[\left\{\frac{1}{f_{p-2}},\frac{1}{f_{p-1}},0,\frac{1}{f_{p+1}},\frac{1}{f_{p+2}}\right\}\right] \tag{74}$$

Small-signal response of the dc-port current is required to define Y_{dd} and can be modeled in the same form as (45). However, the different sequence among the three-phase current and duty ratio responses identified in Table III causes the coefficient matrices to be different. The results are given below in (75). Recall that the dc bus capacitor is excluded from the two-port network. Therefore, this algebraic equation is all we need to represent the dc bus in the power stage model.

$$\hat{\mathbf{i}}_{dc}=\frac{3}{2}\begin{bmatrix}0&0&0&0&0\\0&0&0&0&0\\0&\underline{D}_1&0&\underline{D}_1^*&0\\0&0&0&0&0\\0&0&0&0&0\end{bmatrix}\hat{\mathbf{i}}_a+\frac{3}{2}\begin{bmatrix}0&0&0&0&0\\0&0&0&0&0\\0&\underline{I}_1&0&\underline{I}_1^*&0\\0&0&0&0&0\\0&0&0&0&0\end{bmatrix}\hat{\mathbf{d}}_a \tag{75}$$

With the ac-port voltage unperturbed, the general control model (47) can be reduced to the following, where matrix $\mathbf{Q}$ and $\mathbf{E}$ models ac-port current and dc bus voltage control, respectively:

$$\hat{\mathbf{d}}_a=\mathbf{Q}\hat{\mathbf{i}}_a+\mathbf{E}\hat{\mathbf{v}}_{dc} \tag{76}$$

The basic form of $\mathbf{Q}$ remains the same as in (49), but the diagonal elements have to be refined to reflect the different sequence of each small-signal current:

$$q_k=|\mathrm{mod}(k,3)|\cdot\{\mathrm{mod}(k,3)jK_d-H_i\left[j2\pi\left(f_p+kf_1\right)-mod(k,3)j2\pi f_1\right]\} \tag{77}$$

To define matrix $\mathbf{E}$, refer to Fig. 1 and note first that a dc-port voltage perturbation $\hat{v}_{dc}(f_p)$ produces a perturbation in the d-axis reference current i_{dr}, which in turn causes a perturbation in the d-axis PWM reference m_d, both at the same frequency f_p:

$$\begin{cases}\hat{i}_{dr}\left(f_p\right)=H_v\left(j\omega_p\right)\hat{v}_{dc}\left(f_p\right)\\ \hat{m}_d\left(f_p\right)=H_i\left(j\omega_p\right)\hat{i}_{dr}\left(f_p\right)\end{cases} \tag{78}$$

Since $\hat{v}_{dc}(f_p)$ does not cause a q-axis response, its contribution to PWM references is calculated to be:

$$\begin{bmatrix}\hat{m}_a\\\hat{m}_b\\\hat{m}_c\end{bmatrix}=\frac{1}{\sqrt{6}}\begin{bmatrix}\cos\left(\omega_{p-1}t-\varphi_{v1}\right)\\\cos\left(\omega_{p-1}t-\varphi_{v1}+\frac{2\pi}{3}\right)\\\cos\left(\omega_{p-1}t-\varphi_{v1}-\frac{2\pi}{3}\right)\end{bmatrix}\hat{m}_d\left(f_p\right)+\frac{1}{\sqrt{6}}\begin{bmatrix}\cos\left(\omega_{p+1}t+\varphi_{v1}\right)\\\cos\left(\omega_{p+1}t+\varphi_{v1}-\frac{2\pi}{3}\right)\\\cos\left(\omega_{p+1}t+\varphi_{v1}+\frac{2\pi}{3}\right)\end{bmatrix}\hat{m}_d\left(f_p\right) \tag{79}$$

The first term on the right-hand side of (79) is at frequency f_p-f_1 and is in the negative sequence; the second term is at frequency f_p+f_1 and is in the positive sequence. Note that the sequence of responses at each frequency is consistent with that identified in Table III.

Based on (78) and (79), the contribution of dc bus voltage control to phase-a small-signal duty ratio response can be written in the frequency domain as

$$\frac{K_m}{\sqrt{6}}\begin{bmatrix}0\\e^{-j\varphi_{v1}}H_v\left(j\omega_p\right)H_i\left(j\omega_p\right)\\0\\e^{j\varphi_{v1}}H_v\left(j\omega_p\right)H_i\left(j\omega_p\right)\\0\end{bmatrix}.$$

This leads to the following matrix $\mathbf{E}$ and completes the definition of the frequency-domain control model (76):

$$\mathbf{E}=\frac{K_m}{\sqrt{6}}\begin{bmatrix}0&0&0&0&0\\0&0&e^{-j\varphi_{v1}}H_v\left(j\omega_p\right)H_i\left(j\omega_p\right)&0&0\\0&0&0&0&0\\0&0&e^{j\varphi_{v1}}H_v\left(j\omega_p\right)H_i\left(j\omega_p\right)&0&0\\0&0&0&0&0\end{bmatrix} \tag{80}$$

With the coefficient matrices defined, (73) and (76) can be combined and solved for the ac-port current response $\hat{\mathbf{i}}_a$:

$$\hat{\mathbf{i}}_a=(\mathbf{U}-V_{dc}\mathbf{Y}_{ld}\mathbf{Q})^{-1}\mathbf{Y}_{ld}(V_{dc}\mathbf{E}+\mathbf{D}_a)\hat{\mathbf{v}}_{dc} \tag{81}$$

As can be seen from the definition (58), the second and fourth element of $\hat{\mathbf{i}}_a$ corresponds to small-signal current

$\hat{i}_a(f_p - f_1)$ and $\hat{i}_a(f_p + f_1)$, respectively. Their ratio to the dc-port voltage perturbation $\hat{v}_{dc}(f_p)$ defines the transfer admittances Y_{dn} and Y_{dn}. Other elements of $\hat{\mathbf{i}}_a$ are zero, as expected from the discussion in Subsection II.C.

To find the dc-port current response, (81) is first substituted into (76) to find $\hat{\mathbf{d}}_a$ and then together substituted into (75). The resulting $\hat{\mathbf{i}}_{dc}$ has only one non-zero component, which is the element in the middle of the vector and corresponds to $\hat{i}_{dc}(f_p)$. The ratio of this current to the dc-port voltage perturbation $\hat{v}_{dc}(f_p)$ defines the dc-port admittance Y_{dd}.

Each of the three transfer functions are developed as outlined above and then simplified. The final results are given below in (82)-(84), where P and Q is the active and reactive power output of the converter, respectively, V_1 is the amplitude of the phase voltage, and I_{1d} is the d-axis component of the phase current, i.e., $I_{1d} = I_1 \cos(\varphi_{i1} - \varphi_{v1})$; other variables have been defined and used before.

$$Y_{dd}(s) = \frac{1}{sL + H_{i0}(s)} \left[\frac{3V_1^2}{2V_{dc}^2} + \frac{\omega_1 LQ - H_{i0}(s) P}{V_{dc}^2} + \frac{\sqrt{6} H_{i0}(s) H_v(s)}{2} \frac{V_1 + sLI_{1d}}{V_{dc}} \right] \tag{82}$$

$$Y_{dp}(s) = \frac{\frac{\underline{V}_1 + j\omega_1 L \underline{I}_1}{2V_{dc}} + \frac{1}{\sqrt{6}} H_{i0}(s) H_v(s) e^{j\varphi_{v1}}}{(s + j\omega_1) L + H_{i0}(s) - jK_{d0}} \tag{83}$$

$$Y_{dn}(s) = \frac{\frac{\underline{V}_1^* - j\omega_1 L \underline{I}_1^*}{2V_{dc}} + \frac{1}{\sqrt{6}} H_{i0}(s) H_v(s) e^{-j\varphi_{v1}}}{(s - j\omega_1) L + H_{i0}(s) + jK_{d0}} \tag{84}$$

Note that there is a relationship similar to (69)-(71) between transfer admittances Y_{dp} and Y_{dn}:

$$Y_{dn}(s) = Y_{dp}^*(-s) \tag{85}$$

This can be verified by comparing (83) and (84) and noting that $H_i(s) = H_i^*(-s)$ and $H_v(s) = H_v^*(-s)$. The relationship further reduces the number of mathematically independent models from six to five.

V. VALIDATION AND CHARACTERISTICS

This section presents quantitative results to validate the analytical models developed in the last section. The transfer immittance models are examined to clarify a misconception about sequence coupling. Two simplified versions of the models are presented based on approximations that can be made in different frequency ranges. Adaptation of the models for use with different or additional control functions is also discussed.

A. VALIDATION

The transfer functions developed in the last two sections assumed that the converter is connected to an ideal voltage source at the unperturbed port. This makes it difficult to validate the models by measurement because no practical power sources can meet this requirement. On the other hand, development of the small-signal models essentially consists of two steps: a) mathematical abstraction and approximation of a physical converter by a mathematic model (1)-(2), and b) linearization of the mathematic model. The first step involves various idealization and approximation of actual physical behaviors, but is well established in power electronics and the resulting model (1)-(2) are commonly accepted. The second step is new, hence should be the focus of validation. Because this step builds upon the already-proven large-signal model (1)-(2), it can be performed by comparing the responses of the developed frequency-domain models against that of (1)-(2). Numerical simulation can serve this purpose very well.

Based on these considerations, we have used numerical simulation instead of physical measurement to validate the developed models. The simulation is based on a detailed circuit model using ideal components. To validate each set of transfer functions, the simulation model is set up according to the conditions modeled by each transfer function. A voltage perturbation at a particular frequency is injected after a steady state has been reached, and the simulation continues until it reaches a new periodic steady state. Fourier analysis is then applied to extract the frequency responses modeled by each of the immittance models being validated. The simulation is repeated by varying the perturbation frequency to produce a full scan over the frequency range of interest.

TABLE IV: Parameters and Operation Condition of Example Converter *Con*#1

Parameter	Value	Parameter	Value
L	60 μH	$\underline{V}_1$	563.4∠30°
C_{dc}	10 mF	$\underline{I}_1$	3550∠15°
f_1	60 Hz	V_{dc}	1500 V
f_s	2.5 kHz	K_m	1

Table IV summarizes key component values and operation conditions of the simulated converter, referred to as converter *Con*#1 hereafter. The converter is basically a 3 MVA inverter switching at $f_s = 2.5$ kHz and operating with a 690 V/60 Hz grid. All control loops are designed to have 45° phase margin and with the following crossover frequencies: 300 Hz for ac current control, 15 Hz for PLL, and 10 Hz for dc bus voltage control. The simulated frequency responses are compared to predictions by analytical models.

Fig. 5 compares the responses of the converter to an ac-port voltage perturbation, while responses to a dc-port perturbation are compared in Fig. 6. In both figures, simulation results are marked by points of various shapes and continuous curves are plotted using the analytical models (59)-(61) and (82)-(84).

As can be seen, the responses predicted by each analytical model match the simulation scan results in all cases. The small difference in the phase response of Y_{pn} above 300 Hz is caused by the very small current at the coupling frequency that is difficult to reproduce accurately in simulation. Each of the relationships (69)-(71) between positive- and negative-sequence perturbations is also verified by the same method.

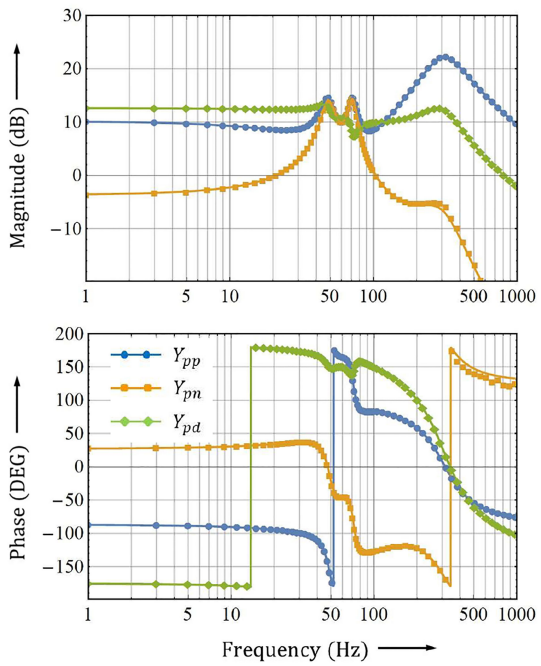

FIGURE 5. **Comparison of responses of transfer functions Y_{pp}, Y_{pd}, and Y_{pn} between analytical models and detailed circuit simulation.**

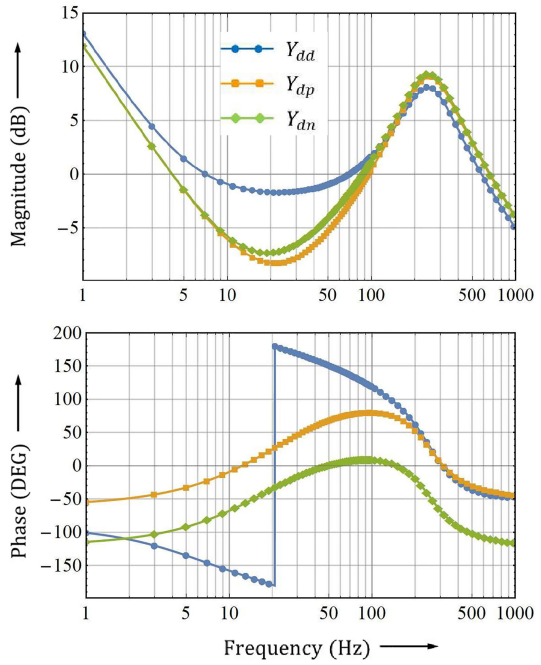

FIGURE 6. **Comparison of responses of transfer functions Y_{dd}, Y_{dp}, and Y_{dn} between analytical models and detailed circuit simulation.**

B. TRANSFER IMMITTANCES AND SEQUENCE COUPLING

Fig. 5 shows that $Y_{pn}(s)$ is comparable to $Y_{pp}(s)$ in their magnitude responses within 10-20 Hz of the fundamental frequency. Outside that frequency range, especially about 100 Hz, $Y_{pn}(s)$ decays rapidly and becomes negligible. This behavior is typical and is related to practical PLL design. As can be seen from (60), $Y_{pn}(s)$ is proportional to the PLL close-loop gain $G_\theta(s - j\omega_1)$. The limited bandwidth of practical PLL designs means that this term is only significant within a narrow frequency range centered at the fundamental. Dc bus voltage control has similar effects and the behavior will be explained in Part II of the paper [37] in conjunction with system stability analysis.

Fig. 6 shows that transfer admittances of the dc port are comparable to the self admittance at all frequencies. The magnitude peaks between 200 Hz and 300 Hz, which corresponds to the current control bandwidth, and then decays as frequency further increases. From the analytical models (83)-(84), it can be seen that both transfer admittances are dominated by the filter inductor L above the current loop crossover frequency, which gives the characteristic 20 dB/decade roll-off in the magnitude response above 300 Hz.

The analytical models also reveal an important feature of the transfer admittances, namely, their phase responses come with an offset that depends on the time of measurement. To explain that, recall the definition of initial phase angles by (28) and note that each angle is measured relative to the time when voltage perturbation is applied. Note also that $\varphi_{i1} - \varphi_{v1}$ and $\varphi_{d1} - \varphi_{v1}$ are defined by the converter design and operation, but φ_{v1} can be arbitrary. Additionally, recall from (34) and (72) that the voltage perturbation was assigned an initial phase angle φ_p but it does not appear in any of the admittance models (59)-(61) and (82)-(84), as expected of small-signal models.

The dc-port self admittance $Y_{dd}(s)$ does not depend on the phase of any ac-port steady state variables. The ac-port self admittance $Y_{pp}(s)$ involves all three phasors defined in (28) but is invariant with respect to the measurement time because it depends on $\varphi_{i1} - \varphi_{v1}$ and $\varphi_{d1} - \varphi_{v1}$, but not φ_{v1} alone. However, that is not the case for the transfer admittances. For example, when the starting point of measurement is shifted over time to cause the voltage phase angle to change from φ_{v1} to $\varphi_{v1} + \Delta\varphi$, phase responses of the transfer admittances will be affected as follows:

- $Y_{pd}(s)$ and $Y_{dn}(s)$ phase is offset by $-\Delta\varphi$
- $Y_{pn}(s)$ phase is offset by $-2\Delta\varphi$
- $Y_{dp}(s)$ phase is offset by $\Delta\varphi$

This dependency can be traced back to the origin of the current response described by each of the transfer admittances. As explained in Sections II and III, a response at each coupling frequency is created when the small-signal component of one variable is multiplied with the steady-state component of another variable through a bilinear term between the two. The initial phase angle of the steady-state variable, which can be the ac port voltage, current or duty ratio, becomes part of the phase of the resulting small-signal variable and carries into the final immittance model, leading to the observed characteristic.

The characteristic discussed above is fundamental to ac-dc converters and has to be considered when using any of the transfer immittance models. To avoid ambiguity and possible misuse, a final system stability model should avoid using the transfer immittance models in a standalone form that may introduce an arbitrariness in the phase response. This will be

an important consideration for the applications presented in Part II of the paper.

The existence of the coupled currents modeled by transfer admittances $Y_{pn}(s)$ and $Y_{np}(s)$ has generated considerable interests as well as confusions in the last few years. Ref. [46] and several other papers treated it as coupling between positive- and negative-sequence dynamics of the converter and proposed to model them together by an admittance matrix, which, using the symbols defined in this paper, is

$$\mathbf{Y}(s) = \begin{bmatrix} Y_{pp}(s) & Y_{np}(s - j2\omega_1) \\ Y_{pn}(s) & Y_{nn}(s - j2\omega_1) \end{bmatrix} \tag{86}$$

To account for this coupling in system stability analysis, [46] proposed to model the grid also in a matrix form as follows, where the diagonal elements are the grid impedance in the positive and negative sequence, and to apply the generalized Nyquist criterion (GNC) to matrix $\mathbf{Z}_g(s)\mathbf{Y}(s)$ to assess system stability:

$$\mathbf{Z}_g(s) = \begin{bmatrix} Z_{gp}(s) & 0 \\ 0 & Z_{gn}(s - j2\omega_1) \end{bmatrix} \tag{87}$$

There are several issues with this formulation and stability analysis method. First, direct use of the admittance matrix (86) in a stability model is problematic because of the arbitrariness associated with phase responses of the diagonal elements. While the phase dependency of Y_{np} and Y_{pn} on φ_{v1} cancels out in the eigenvalues of $\mathbf{Z}_g(s)\mathbf{Y}(s)$ when $\mathbf{Z}_g(s)$ is diagonal, as assumed in (87), such that this may appear to be just an issue of notation, the cancellation will not happen and the phase response of each eigenvalue of $\mathbf{Z}_g(s)\mathbf{Y}(s)$ will have a degree of arbitrariness if the grid impedance is also coupled between the positive and negative sequence. The matrix formulation also necessitates the GNC to determine stability, taking away the simplicity, intuitiveness as well as the ability to develop general conclusions using analytical models offered by the original impedance-based method [27].

Treating the coupled currents as the results of sequence coupling is also a mischaracterization of the phenomenon which in actuality is a coupling over frequency. It may appear as sequence coupling because of the difference in the sequence of the perturbation and the resulting coupled current response. However, as discussed in Section IV.D, the association of a set of small-signal variables with a sequence is not unique. For example, the negative-sequence currents at frequency $f_p - 2f_1$ modeled by transfer admittance $Y_{pn}(s)$ can also be treated as positive-sequence currents at $2f_1 - f_p$. In fact, for $f_p < 2f_1$, it is conceptually more convenient to treat the currents as positive sequence at a positive frequency $2f_1 - f_p$. Practically, $2f_1$ is also the upper boundary of the frequency range in which coupling impacts system stability. Therefore, the term *sequence coupling* on which (86) is based is ambiguous and does not reflect the actual nature of the coupling.

The matrix form (86) has also led to the notion that sequence impedances must be somehow related to dq-frame impedances such that one can be developed from the other. Several papers have tried to establish such a relationship. For example, [49] defined a so-called modified sequence-domain impedance matrix, which is essentially (86) in impedance form, and suggested that it could be related to the dq-frame impedance matrix by a constant matrix. Similar relationship was presented in [50] using $\alpha\beta$-frame instead of sequence variables. Common to these works and [46] are:

- The assumption that the dc bus is an ideal voltage source, such that PLL is the only nonlinearity that contributes to the coupled current; and
- The formulation of a system impedance model in the form of a 2×2 matrix to which the GNC is applied to determine system stability.

Given the fundamental difference in the principles based on which sequence-domain and dq-frame immittance models are developed, as discussed in Section II, it is questionable that there is a general mathematical relationship between the two types of models. This question arises naturally if one considers the cases identified in Section II (unbalanced, distorted, etc.) where the dq-frame method fails but harmonic linearization can still work. If there were a general relationship between the two such that dq-frame immittances could be derived indirectly from sequence immittance models, why cannot they be developed directly in principle? Nevertheless, looking for such a relationship may still be a worthwhile effort, as the process itself may offer more insights about each of the methods. On the other hand, such effort should be based on general principles instead of a case study, and avoid overgeneralizing from some special cases, such as ignoring dc bus dynamics.

C. MODEL REDUCTION

The models presented in the last section are general and include all relevant factors. The analytical form makes them easy to use and gain insight from. The models also share some common structure that shows how different control functions affect the impedance. Since each control function is active only in a particular frequency range, it may be ignored in other frequency ranges to simplify the models. This subsection presents such simplified models according to the frequency range of interest.

One common term that appears in the models (59)-(61) and (82)-(84) is $sL + [H_{i0}(s - j\omega_1) - jK_{d0}]$ (and some variation of it). This is in fact the positive-sequence impedance of the converter when no PLL is used and when the dc bus can be treated as an ideal voltage source [23]. Recall the definition of K_{d0} from (62). When the current control decoupling gain K_d is selected to cancel the coupling term between d- and q-axis, we have $K_{d0} = \omega_1 L$. This will be assumed for all the approximate models presented in this subsection, under which the term mentioned above can be written as follows:

$$sL + \left[H_{i0}(s - j\omega_1) - jK_{d0}\right] = (s - j\omega_1)L + H_{i0}(s - j\omega_1)$$

The PLL is usually designed to have a bandwidth no more than 20-30 Hz. Therefore, the PLL close-loop gain $G_\theta(s)$ can be set to zero at high frequency. There is a similar limit on

the bandwidth of dc bus voltage control, such that $H_v(s)$ can also be set to zero at high frequency. Applying these to (59)-(61) and (82)-(84), we obtain the following high-frequency (indicated by adding "$-h$" to the subscript) simplified models:

$$Y_{pp-h}(s) = \frac{1}{(s-j\omega_1)L + H_{i0}(s-j\omega_1)} \tag{88}$$

$$Y_{pn-h}(s) = -\frac{\underline{I}_1^* G_\theta(s-j\omega_1)}{2\underline{V}_1} \approx 0 \tag{89}$$

$$Y_{pd-h}(s) = \frac{3}{2V_{dc}} \frac{\underline{V}_1^* - \underline{I}_1^* H_{i0}(s-j\omega_1)}{H_{i0}(s-j\omega_1) + (s-j\omega_1)L} \tag{90}$$

$$Y_{dp-h}(s) = \frac{\underline{D}_1}{2} \cdot \frac{1}{sL + H_{i0}(s)} \tag{91}$$

$$Y_{dn-h}(s) = \frac{\underline{D}_1^*}{2} \cdot \frac{1}{sL + H_{i0}(s)} \tag{92}$$

$$Y_{dd-h}(s) = \frac{V_{dc}^{-2}}{sL + H_{i0}(s)} \left[\omega_1 LQ - H_{i0}(s) P + \frac{3V_1^2}{2} \right] \tag{93}$$

Note that models (88)-(90) also represent the exact form of Y_{pp}, Y_{pn} and Y_{pd} for converters that do not use a PLL. Similarly, (91)-(93) represent the exact Y_{dp}, Y_{dn} and Y_{dd} models for converters not equipped with dc bus voltage control, e.g., the generator-side converter in a type-IV turbine.

To simplify (59)-(61) and (82)-(84) at low frequency, we can ignore terms like sL and $(s-j\omega_1)L$ that are added to $H_{i0}(s)$ or $H_{i0}(s-j\omega_1)$ because $H_{i0}(s) \gg sL$ holds within the current control bandwidth. Accordingly, the following low-frequency approximate models are developed, where $\underline{S} = P + jQ$ is the apparent power output of the converter, and the added subscript "$-l$" indicates low frequency:

$$Y_{pp-l}(s) = \frac{1}{H_{i0}(s-j\omega_1)} - \frac{\underline{I}_1 G_\theta(s-j\omega_1)}{2\underline{V}_1} \tag{94}$$

$$Y_{pn-l}(s) = -\frac{\underline{I}_1^* G_\theta(s-j\omega_1)}{2\underline{V}_1} \tag{95}$$

$$Y_{pd-l}(s) = \frac{3\underline{V}_1^*/(2V_{dc})}{H_{i0}(s-j\omega_1)} - \frac{\underline{S} - jQG_\theta(s-j\omega_1)}{\underline{V}_1 V_{dc}} \tag{96}$$

$$Y_{dp-l}(s) = \frac{\underline{D}_1}{2} \cdot \frac{1}{H_{i0}(s)} + \sqrt{\frac{1}{6}} H_v(s) e^{j\varphi_{v1}} \tag{97}$$

$$Y_{dn-l}(s) = \frac{\underline{D}_1^*}{2} \cdot \frac{1}{H_{i0}(s)} + \sqrt{\frac{1}{6}} H_v(s) e^{-j\varphi_{v1}} \tag{98}$$

$$Y_{dd-l}(s) = \frac{\sqrt{6}H_v(s)}{2} \frac{V_1}{V_{dc}} + \frac{3V_1^2}{2V_{dc}^2} \frac{1}{H_{i0}(s)} - \frac{P}{V_{dc}^2} \tag{99}$$

In general, the low-frequency models are accurate up to 100-150 Hz, above which the high-frequency models can be used. For easy reference, we consider the second harmonic frequency ($2f_1$) to be the boundary between the two frequency ranges. The bandwidth limits discussed before for PLL and dc bus voltage control are for 50/60 Hz power grid applications and can be proportionally higher if the fundamental frequency is higher, e.g., in aircraft power systems that use 400 Hz or variable-frequency ac. Therefore, the boundary between the low and high frequency ranges depends on the fundamental and specifying it by the second harmonic frequency instead of a fix value makes the definition more general.

D. OTHER CONSIDERATIONS

The analytical models have been developed by assuming the specific control architecture of the converter defined in Fig. 1. Since the models depend strongly on control design that may be different in different applications, it is important to consider how the models may be adapted for converters that use different control design.

Of the three control functions considered in Fig. 1, ac phase current control is essential for voltage-source converters and dq-frame control is preferred because of its ability to eliminate steady-state error. The dq-frame current compensator $H_i(s)$ is usually a PI regulator but may include additional transfer function blocks in series or parallel to provide damping at certain frequency or to improve other aspects of control performance. Such additional blocks may be modeled together with the basic PI compensator and their collective transfer function be used in place of $H_i(s)$ in each of the developed models. It does not affect other aspects of the models.

In the positive-sequence models (59)-(61), the frequency appearing in the current compensator transfer function is shifted from the frequency of perturbation down by the fundamental. This is necessary when dq transformation is involved because it changes the frequency of three-phase signals at frequency f to $f - f_1$ if the signals are in positive sequence and to $f + f_1$ if the signals are in negative sequence. Such frequency shift does not appear when stationary-frame current control is used. Therefore, to use the developed models in that case, one can simply replace $H_{i0}(s-j\omega_1)$ in (59)-(61) by $H_{i0}(s)$. Similar changes can be made to the negative-sequence models.

DC bus voltage control is an integral part of standalone VSCs. It affects the dc-port transfer functions (82)-(84) but the models do not depend on the specific form of the compensator. Therefore, the models can be used as long as the control can be represented by a transfer function $H_v(s)$. This also includes the possible use of nonlinear control, which can be linearized to define an equivalent small-signal transfer function. For converters that are not equipped with dc bus voltage control, for example the generator-side converter in a type-IV turbine or the sending end of an HVDC transmission line, the developed models can be used with $H_v(s)$ set to zero, which essentially become the high-frequency approximate models (91)-(93).

The PLL, or grid synchronization in general, is a function that has seen the most variation in practice and is still evolving. The models were developed by assuming a basic design that locks to the positive-sequence component of the grid voltage. To see how the models can be adapted when a different PLL design is used, note first that, although the intermediate steps involve PLL internal design, the final model

only depends on its close-loop transfer function $G_\theta(s)$. Note also that the only term related to the PLL that appears in the models is

$$\frac{G_\theta\left(s-j\omega_1\right)}{\underline{V}_1}. \tag{100}$$

Further analysis of the PLL model indicates that (100) is actually the transfer function from the grid voltage to the cosine of the PLL output when the grid voltage contains a positive-sequence perturbation. Therefore, to use the developed models for converters employing a different PLL design, one only needs to remodel the PLL to determine its transfer function as defined below where $\hat{v}_a$ is the voltage perturbation and $\hat{\theta}$ is the resulting angle response:

$$\frac{\cos\hat{\theta}\left(s-j\omega_1\right)}{\hat{v}_a\left(s\right)} \triangleq \Gamma\left(s\right) \tag{101}$$

For a PLL that responds to positive- and negative-sequence perturbation differently, $\Gamma(s)$ depends on the sequence and can be denoted as $\Gamma_p(s)$ and $\Gamma_n(s)$, respectively. Once these transfer functions are developed, $\Gamma_p(s)$ can be used in place of (100) in (59)-(61), and the results are Y_{pp}, Y_{pn} and Y_{pd} of the converter. Similarly, $\Gamma_n(s)$ can be used in place of $G_\theta(s+j\omega_1)/\underline{V}_1^*$ in the negative-sequence model to define Y_{nn}, Y_{np} and Y_{nd} of the converter.

In addition to the three control functions modeled in this work, a converter connected to the power grid may also be equipped with ac voltage control that regulates the voltage at the point of interconnect (POI). The control models provided in Section IV can be modified to include this and any additional converter-level control function.

The models developed so far have assumed a first-order inductive filter at the ac terminal of the converter. Additional filter elements, such as shunt filter capacitors, can be included when performing system stability analysis. On the other hand, the filter capacitor impedance is usually more than an order of magnitude higher than the grid impedance below the second harmonic frequency even in a very weak grid. Therefore, they can be neglected in system stability analysis below the second harmonic frequency in which the coupling effects have to be considered. Above the second harmonic frequency, the coupling effects can be ignored and it is rather straightforward to include additional filter components in the self-admittances of the ac port.

VI. SUMMARY

An ac-dc converter can be described as a two-port network and modeled by a set of self and transfer immittances for use in system stability analysis. The additional degree of freedom at the ac terminal due to three-phase operation is represented by the sequence of ac-port variables. A self immittance is used to model the relationship between small-signal voltage and current of the same port at the same frequency (and the same sequence in the case of ac port). Two types of transfer immittances are used to model the coupling across the two ports as well as that over frequency. The coupling over frequency is unique to ac-dc converters and involves a frequency shift by two times the fundamental. The coupling between the two ports resembles that of traditional two-port networks but is sequence-dependent and also involves a frequency shift. Altogether, three self immittances and six transfer immittances are defined to fully characterize the converter in the frequency domain. Of them, three are made mathematically redundant by a general relationship between positive and negative sequence models such that only six need to be actually modeled.

The method to model the self and transfer immittances is based on multi-harmonic linearization. Each immittance is modeled in an analytical form and the models are validated against frequency scan based on detailed circuit simulation. Characteristics of the transfer immittances, especially the ones describing coupling over frequency are examined to clarify a misinterpretation promulgated by several recent publications and to shed light on proper use of the models. The four transfer immittances describing the coupling between the ac and dc ports provide new insights about ac-dc converters and their effects on the system they connect to at the ac and ac terminals.

The developed immittance models provide a general framework to study small-signal stability of renewable energy, high-voltage dc transmission, as well general ac, dc and hybrid ac-dc power systems that involve ac-dc converters. Part II of the paper [37] will present these applications.

REFERENCES

[1] R. D. Middlebrook, "Input filter considerations in design and application of switching regulators," in *Proc. IEEE IAS Annu. Meeting*, 1976, pp. 366–382.

[2] B. H. Cho and F. C. Lee, "Modeling and analysis of spacecraft power systems," *IEEE Trans. Power Electron.*, vol. 3, no. 1, pp. 44–54, Jan. 1988.

[3] C. M. Wildrick, F. C. Lee, B. H. Cho, and B. Choi, "A method of defining the load impedance specification for a stable distributed power system," *IEEE Trans. Power Electron.*, vol. 10, no. 3, pp. 280–285, May 1995.

[4] X. Lu, K. Sun, J. M. Guerrero, J. C. Vasquez, L. Huang, and J. Wang, "Stability enhancement based on virtual impedance for DC microgrids with constant power loads," *IEEE Trans. Smart Grid*, vol. 6, no. 6, pp. 2770–2783, Nov. 2015.

[5] J. Sun, "Input impedance analysis of single-phase PFC converters," *IEEE Trans. Power Electron.*, vol. 20, no. 2, pp. 308–314, Mar. 2005.

[6] M. Belkhayat, *Stability Criteria for AC Power Systems With Regulated Loads*, Ph.D. dissertation, Elect. Comp. Eng., Purdue Univ., West Lafayette, IN, USA, 1997.

[7] H. Mao, D. Boroyevich, and F. C. Lee, "Novel reduced-order small-signal model of a three-phase PWM rectifier and its application in control design and system analysis," *IEEE Trans. Power Electron.*, vol. 13, no. 3, pp. 511–521, May 1998.

[8] J. Sun, "Small-signal methods for ac distributed power systems – A review," *IEEE Trans. Power Electron.*, vol. 24, no. 11, pp. 2545–2554, Nov. 2009.

[9] L. M. Hajagos and B. Danai, "Laboratory measurements and models of modern loads and their effect on voltage stability studies," *IEEE Trans. Power Syst.*, vol. 13, no. 2, pp. 584–592, May 1998.

[10] M. Rylander, W. M. Grady, A. Arapostathis, and E. J. Powers, "Power electronic transient load model for use in stability studies of electric power grids," *IEEE Trans. Power Syst.*, vol. 25, no. 2, pp. 914–921, May 2010.

[11] J. Sun, M. Xu, M. Cespedes, D. Wong, and M. Kauffman, "Modeling and analysis of data center power system stability by impedance methods," in *Proc. IEEE Energy Convers. Congr. Expo.*, Oct. 2019, pp. 1–10.

[12] R-I-29995, *Anforderungen an die Eingangs-Admittanz von Umrichtertriebfahrzeugen*, SBB, May 2009.
[13] S. Menth and M. Meyer, "Low frequency power oscillations in electric railway systems," *Elektrische Bahnen*, vol. 104, no. 4, pp. 216–221, 2006.
[14] P. Pan, H. Hu, X. Yang, F. Blaabjerg, X. Wang, and Z. He, "Impedance measurement of traction network and electric train for stability analysis in high-speed railways," *IEEE Trans. Power Electron.*, vol. 33, no. 12, pp. 10086–10100, Dec. 2018.
[15] C. Buchhagen, M. Greve, A. Menze, and J. Jung, "Harmonic stability – practical experience of a TSO," in *Proc. Wind Integr. Workshop*, Nov. 2016, pp. 1–6.
[16] H. Saad, Y. Fillion, S. Deschanvres, Y. Vernay, and S. Dennetiere, "On resonances and harmonics in HVDC-MMC station connected to ac grid," *IEEE Trans. Power Del.*, vol. 32, no. 3, pp. 1565–1573, Jun. 2017.
[17] J. Sun *et al.*, "Renewable energy transmission by HVDC across the continent: System challenges and opportunities," *CSEE J. Power Energy Syst.*, vol. 3, no. 4, pp. 353–364, Dec. 2017.
[18] C. Zou *et al.*, "Analysis of resonance between a VSC-HVDC converter and the ac grid," *IEEE Trans. Power Electron.*, vol. 33, no. 12, pp. 10157–10168, Dec. 2018.
[19] U. N. Gnanarathna, A. M. Gole, and R. P. Jayasinghe, "Efficient modeling of modular multilevel HVDC converters (MMC) on electromagnetic transient simulation programs," *IEEE Trans. Power Del.*, vol. 26, no. 1, pp. 316–324, Jan. 2011.
[20] W. Dong, H. Xin, D. Wu, and L. Huang, "Small-signal stability analysis of multi-infeed power electronic systems based on grid strength assessment," *IEEE Trans. Power Syst.*, vol. 34, no. 2, pp. 1391–1403, Mar. 2019.
[21] C. Zhang, M. Molinas, A. Rygg, and X. Cai, "Impedance-based analysis of interconnected power electronics systems: Impedance network modeling and comparative studies of stability criteria," *IEEE J. Emerg. Sel. Topics Power Electron.*, vol. 8, no. 3, pp. 2520–2533, Sep. 2020.
[22] I. Vieto and J. Sun, "On system modeling and analysis using DQ-frame impedance models," in *Proc. IEEE 18th Workshop Control Model. Power Electron.*, Jul. 2017, pp. 1–8.
[23] M. Cespedes and J. Sun, "Impedance modeling and analysis of grid-connected voltage-source converters," *IEEE Trans. Power Electron.,* vol. 29, no. 3, pp. 1254–1261, Mar. 2014.
[24] W. Ren and E. Larsen, "A refined frequency scan approach to subsynchronous control interaction (SSCI) study of wind farms," *IEEE Trans. Power Syst.*, vol. 31, no. 5, pp. 3904–3912, Sep. 2016.
[25] G. Li and J. Sun, "Control hardware-in-the-loop simulation for turbine impedance modeling and verification," in *Proc. Wind Integration Workshop*, Oct. 2017, pp. 1–6.
[26] W. Liu, X. Xie, X. Zhang, and X. Li, "Frequency-coupling admittance modeling of converter-based wind turbine generators and the control-hardware-in-the-loop validation," *IEEE Trans. Energy Convers.*, vol. 35, no. 1, pp. 425–433, Mar. 2020.
[27] J. Sun, "Impedance-based stability criterion for grid-connected inverters," *IEEE Trans. Power Electron.*, vol. 26, no. 11, pp. 3075–3078, Nov. 2011.
[28] J. J. Grainger and W. D. Stevenson, *Power System Analysis*. New York, NY, USA: McGraw-Hill, 1994.
[29] I. Vieto and J. Sun, "Sequence impedance modeling and analysis of type-III wind turbines," *IEEE Trans. Energy Convers.*, vol. 33, no. 2, pp. 537–545, Jun. 2018.
[30] A. A. A. Radwan and Y. A. I. Mohamed, "Assessment and mitigation of interaction dynamics in hybrid ac/dc distribution generation systems," *IEEE Trans. Smart Grid*, vol. 3, no. 3, pp. 1382–1393, Sep. 2012.
[31] G. Pinares and M. Bongiorno, "Modeling and analysis of VSC-based HVDC systems for dc network stability studies," *IEEE Trans. Power Del.*, vol. 31, no. 2, pp. 848–856, Apr. 2016.
[32] Y. Song and C. Breitholtz, "Nyquist stability analysis of an ac-grid connected VSC-HVDC system using a distributed parameter DC cable model," *IEEE Trans. Power Del.*, vol. 31, no. 2, pp. 898–907, Apr. 2016.
[33] A. M. I. Mohamad and Y. A. I. Mohamed, "Impedance-based analysis and stabilization of active DC distribution systems with positive feedback islanding detection schemes," *IEEE Trans. Power Electron.*, vol. 33, no. 11, pp. 9902–9922, Nov. 2018.
[34] H. Zhang, M. Mehrabankhomartash, M. Saeedifard, Y. Zou, Y. Meng, and X. Wang, "Impedance analysis and stabilization of point-to-point HVDC systems based on a hybrid ac/dc impedance model," *IEEE Trans. Ind. Electron.*, vol. 68, no. 4, pp. 3224–3238, Apr. 2020.
[35] I. Vieto, X. Du, H. Nia, and J. Sun, "Frequency-domain coupling in two-level VSC small-signal dynamics," in *Proc. IEEE 18th Workshop Control Model. Power Electron.*, Jul. 2017, pp. 1–8.
[36] H. W. Bode, *Network Analysis and Feedback Amplifier Design, Princeton: Van Nostran*, Princeton, NJ, USA: Princeton Univ. Press, 1945.
[37] J. Sun, "Two-port characterization and transfer immittances of ac-dc converters—Part II: Applications," *IEEE Open J. Power Electron.*, to be published, doi: 10.1109/OJPEL.2021.3104496.
[38] J. Sun and H. Liu, "Sequence impedance modeling of modular multilevel converters," *IEEE J. Emerg. Sel. Topics Power Electron.*, vol. 5, no. 4, pp. 1427–1443, Dec. 2017.
[39] I. Vieto and J. Sun, "Sequence impedance modeling and converter-grid resonance analysis considering dc bus dynamics and mirrored harmonics," in *Proc. IEEE 19th Workshop Control Model. Power Electron.*, Jun. 2018, pp. 1–8.
[40] I. Vieto and J. Sun, "Prediction of SSR in type-III wind turbines connected to series compensated grids," in *Proc. Wind Integration Workshop*, Oct. 2015, pp. 1–6.
[41] Z. Miao, "Impedance-model-based SSR analysis for type 3 wind generator and series-compensated network" *IEEE Trans. Energy Convers.*, vol. 27, no. 4, pp. 984–991, Dec. 2012.
[42] S. Chernet and M. Bongiorno, "Input impedance based Nyquist stability criterion for subsynchronous resonance analysis in DFIG based wind farms," in *Proc. IEEE Energy Convers. Congr. Expo.,* 2015, pp. 6285–6292.
[43] I. Vieto, S. Rogalla, and J. Sun, "On the potential of subsynchronous resonance of voltage-source converters with the grid," in *Proc. Wind Integration Workshop*, Oct. 2015, pp. 1–7.
[44] Y. Xu, M. Zhang, L. Fan, and Z. Miao, "Small-signal stability analysis of type-4 wind in series-compensated networks," *IEEE Trans. Energy Convers.*, vol. 35, no. 1, pp. 529–538, Mar. 2020.
[45] A. J. Agbemuko, J. L. Domínguez-García, and O. Gomis-Bellmunt, "Impedance-based modelling of a hybrid ac/dc grid with Z-bus approach," in *Proc. IEEE Power Energy Soc. Gen. Meeting*, 2018, pp. 1–5.
[46] M. K. Bakhshizadeh *et al.*, "Couplings in phase domain impedance modeling of grid-connected converters," *IEEE Trans. Power Electron.*, vol. 31, no. 10, pp. 6792–6796, Oct. 2016.
[47] R. A. Horn and C. R. Johnson, *Matrix Analysis*. Cambridge, U.K.: Cambridge Univ. Press, 1985.
[48] A. Gelb and W. E. Vander Velde, *Multiple-Input Describing Functions and Nonlinear System Design*. New York, NY, USA: McGraw-Hill Book, 1968.
[49] A. Rygg, M. Molinas, C. Zhang, and X. Cai, "A modified sequence-domain impedance definition and its equivalence to the dq-domain impedance definition for the stability analysis of ac power electronic systems," *IEEE J. Emerg. Sel. Topics Power Electron.*, vol. 4, no. 4, pp. 1383–1396, Dec. 2016.
[50] X. Wang, L. Harnefors, and F. Blaabjerg, "Unified impedance model of grid-connected voltage-source converters," *IEEE Trans. Power Electron*, vol. 33, no. 2, pp. 1775–1787, Feb. 2018.